# SYS-1/beta-catenin inheritance and regulation by Wnt-signaling during asymmetric cell division.

**Maria F. Valdes Michel[1] and Bryan T. Phillips[1,2*]**

**[1] Interdisciplinary Graduate Program in Genetics, University of Iowa, Iowa City, IA.**

**[2] Department of Biology, University of Iowa, Iowa City IA.**

***Corresponding author**
**Email: bryan-phillips@uiowa.edu**

**Key words: Wnt, SYS-1, beta-catenin, asymmetric cell division, *C. elegans,* APC**

Abstract

Asymmetric cell division (ACD) allows daughter cells of a polarized mother to acquire different developmental fates. In *C. elegans*, the Wnt/β-catenin Asymmetry (WβA) pathway oversees many embryonic and larval ACDs; here, a Wnt gradient induces an asymmetric distribution of Wnt signaling components within the dividing mother cell. One terminal nuclear effector of the WβA pathway is the transcriptional activator SYS-1/β-catenin. SYS-1 is sequentially negatively regulated during ACD; first by centrosomal regulation and subsequent proteasomal degradation and second by asymmetric activity of the β-catenin "destruction complex" in one of the two daughter cells, which decreases SYS-1 levels in the absence of WβA signaling. However, the extent to which mother cell SYS-1 influences cell fate decisions of the daughters is unknown. Here, we quantify inherited SYS-1 in the differentiating daughter cells and the role of SYS-1 inheritance in Wnt-directed ACD. Photobleaching experiments demonstrate the GFP::SYS-1 present in daughter cell nuclei is comprised of inherited and *de novo* translated SYS-1 pools. We used a photoconvertible DENDRA2::SYS-1, to directly observe the dynamics of inherited SYS-1. Photoconversion during mitosis reveals that SYS-1 clearance at the centrosome preferentially degrades older SYS-1, and this accumulation is regulated via dynein trafficking. Photoconversion of the EMS cell during Wnt-driven ACD shows daughter cell inheritance of mother cell SYS-1. Additionally, loss of centrosomal SYS-1 increased inherited SYS-1 and, surprisingly, loss of centrosomal SYS-1 also resulted in increased levels of *de novo* SYS-1 in both EMS daughter cells. Lastly, we show that daughter cell negative regulation of SYS-1 via the destruction complex member APR-1/APC is key to limit both the *de novo* and the inherited SYS-1 pools in both the E and the MS cells. We conclude that regulation of both inherited and newly translated SYS-1 via centrosomal processing in the mother cell and daughter cell regulation via Wnt signaling are critical to maintain sister SYS-1 asymmetry during ACD.

## Introduction

Asymmetric cell division (ACD) is an essential mechanism that controls cell fate specification during development and adult tissue homeostasis. ACD increases the developmental cell diversity needed for functional tissues, including such diverse and well-studied examples as *C. elegans* embryos, *Drosophila* neuroblasts, and mammalian lung epithelial cells (BERTRAND AND HOBERT 2009; NEUMÜLLER AND KNOBLICH 2009; CHHABRA AND BOOTH 2021; KOCHENDOERFER *et al.* 2021). During adulthood, ACD maintains tissue integrity by promoting stem cell self-renewal while also producing cells that will further differentiate to repopulate dying or degraded tissues (YAMASHITA *et al.* 2010). Given that ACDs of stem cells maintain the ability to replenish damaged or growing tissues even post-development, tight regulation of these stem cell niches is needed to prevent tumorigenesis. Accordingly, when pathways that regulate ACD go awry, the risk of cancer increases (MORRISON AND KIMBLE 2006). Both tumorigenesis and development use self-renewal and proliferation to drive progression, which often occurs via regulation of the same signaling pathways. Thus, understanding the mechanism regulating ACDs will contribute to the understanding of how cell fate specification occurs during development and will illuminate the mechanism by which tumors develop (BAJAJ *et al.* 2015).

The Wnt/β-catenin pathway is a well-conserved signaling pathways that regulate stem cell maintenance, cell renewal and differentiation, cell polarity, and ACD (RING *et al.* 2014; CHEN *et al.* 2022; HABIB AND ACEBRÓN 2022; HAYAT *et al.* 2022). In this pathway, Wnt ligands activate a signal transduction cascade that stabilizes the coactivator β-catenin. Stabilized β-catenin translocates into the nucleus which initiates transcription of Wnt target genes. In the absence of Wnt ligand, β-catenin is degraded by a "destruction complex" which is comprised of casein kinase 1α (CK1α), glycogen synthase kinase 3β (GSK3β), and two scaffolds, Axin and adenomatous polyposis coli (APC). Without β-catenin in the nucleus, the transcription factor T-cell factor (TCF) acts as a transcriptional repressor of Wnt-target genes (LIN *et al.* 1998; MACDONALD *et al.* 2009; MURGAN *et al.* 2015). Because the Wnt/β-catenin signaling pathway plays a critical role in cell polarity, ACD, development, and organismal homeostasis, mutations and misregulation of this pathway lead to cell fate dysregulation. Aberrant regulation of Wnt signaling is a common theme of cancer biology. Hyperactivation of Wnt signaling often leads to

107 malignant transformation (DE LA ROCHE *et al.* 2008; POLAKIS 2012). Tumor sequencing further reveals
108 frequent inactivating mutations in APC and activating mutations in β-catenin(GILES *et al.* 2003;
109 OBRADOR-HEVIA *et al.* 2010; QU *et al.* 2016). Constitutive Wnt pathway activity is present in 90% of
110 colorectal cancer cases. This may be impacted by changes in the cell polarity and in ACD, which leads to
111 an increase in the cellular proliferation of the epithelial stem cell population of the intestine (GILES *et al.*
112 2003; QUYN *et al.* 2010). Even though regulation of β-catenin is essential for proper Wnt signaling, how
113 the mother cell distributes β-catenin into the daughter cells and how β-catenin is differentially regulated
114 during ACD remains unclear.

115 *C. elegans* is an excellent model organism to uncover the mechanisms by which the Wnt/β-
116 catenin signaling pathway regulates ACDs. The Wnt/β-catenin asymmetry (WβA) pathway oversees
117 many embryonic and larval ACDs through regulation of the *C. elegans* β-catenin, SYS-1 (KIDD *et al.*
118 2005; HUANG *et al.* 2007; PHILLIPS AND KIMBLE 2009). The WβA pathway is a branched pathway
119 specialized for ACD that uses a β-catenin paralog, WRM-1 and SYS-1, in each branch (ROCHELEAU *et al.*
120 1999; LO *et al.* 2004; KIDD *et al.* 2005; PHILLIPS *et al.* 2007; SUGIOKA *et al.* 2011; ROBERTSON AND LIN
121 2012). One branch activates the nuclear export of approximately 50% of the TCF/LEF DNA-binding
122 protein, POP-1, via association with WRM-1 (LO *et al.* 2004). WRM-1-assisted export of POP-1 is,
123 counterintuitively, required for Wnt-target gene activation likely because POP-1 functions as a
124 transcriptional repressor when not bound to β-catenin/SYS-1 (ROCHELEAU *et al.* 1999; LO *et al.* 2004).
125 POP-1 nuclear export enables the remaining nuclear POP-1 to form a complex with its coactivator β-
126 catenin/SYS-1 (KIDD *et al.* 2005; YANG *et al.* 2015). The second branch of the WβA pathway regulates
127 the stabilization and subsequent nuclear localization of SYS-1, in which SYS-1 ultimately controls
128 transcription of Wnt-target genes by complexing with POP-1 (MIZUMOTO AND SAWA 2007; BALDWIN AND
129 PHILLIPS 2014).

130 SYS-1 is broadly expressed at the transcriptional level but expression, including asymmetric
131 expression, is tightly regulated at the protein level (HUANG *et al.* 2007; PHILLIPS *et al.* 2007). One
132 example of regulation of SYS-1 protein expression is via centrosomal localization and subsequent
133 turnover. SYS-1 symmetrically localizes to the centrosomes during ACD, and that SYS-1 centrosomal

134 localization is dependent on the centrosomal protein, regulator of spindle assembly 2 (RSA-2) (HUANG *et*
135 *al.* 2007; PHILLIPS *et al.* 2007; SCHLAITZ *et al.* 2007; CHRISTIAN 2012; VORA AND PHILLIPS 2015; VORA AND
136 PHILLIPS 2016). RSA-2 depletion demonstrates that RSA-2 is required for SYS-1 centrosomal localization
137 in embryonic mother cells (VORA AND PHILLIPS 2015; VORA AND PHILLIPS 2016). After ACD, overall SYS-1
138 protein levels, including nuclear SYS-1, increase in both daughter cells in the absence of RSA-2. The
139 increase of overall SYS-1 after RSA-2 depletion suggests centrosomal regulation leads to the negative
140 regulation and subsequent degradation of centrosomally localized SYS-1. Thus, negative regulation of
141 SYS-1 via centrosomal localization normally limits the levels of SYS-1 in the daughter cells resulting from
142 an ACD. Depletion of the proteasome core ATPase subunit of the 26S proteasome, RPT-4, results in
143 elevated and stabilized centrosomal SYS-1 and decreased SYS-1 turnover compared to wild type (VORA
144 AND PHILLIPS 2015; VORA AND PHILLIPS 2016). These results are consistent with the hypothesis that the
145 centrosomal proteasome plays a key role in regulating SYS-1 turnover at the centrosome via active
146 degradation by the proteasome.
147 The microtubule motor dynein enhances the rapid accumulation of SYS-1 on mitotic centrosomes
148 of large embryonic blastomeres via microtubule trafficking of SYS-1 (THOMPSON *et al.* 2022), leading to
149 SYS-1 mitotic turnover. Thus, dynein works as a negative regulator of ACD, by enhancing centrosomal
150 SYS-1 levels and subsequent SYS-1 degradation by the centrosomal proteasome. Knockdown of single
151 dynein subunits, including heavy chain DHC-1 or the light chain subunits DLC-1 and DYLT-1, lead to
152 reduced SYS-1 centrosomal enrichment and elevated SYS-1 in both daughter cells. Additionally, loss of
153 these dynein complex subunits results in the conversion of larval ACDs to symmetric divisions,
154 increasing the Wnt-signaled cell fates (THOMPSON *et al.* 2022). These data highlight the importance of
155 microtubule trafficking for SYS-1 centrosomal localization and subsequent degradation. However, when
156 treating embryos with the drug nocodazole to disable microtubule polymerization and subsequent
157 microtubule trafficking, a surprising increase of cytoplasmic and centrosomal SYS-1 was observed, in
158 addition to a less mobile SYS-1 compared to wild type (THOMPSON *et al.* 2022). These data, therefore,
159 suggest that a negative regulator of SYS-1 is also trafficked to the centrosome by the dynein motor that
160 regulates SYS-1 levels. The nocodazole phenotype is similar to that of RPT-4 depletion, which also

161 resulted in elevated centrosomal SYS-1 (VORA AND PHILLIPS 2015; VORA AND PHILLIPS 2016), indicating
162 that the trafficked negative regulator may be the proteasome itself. Strengthening this hypothesis, when
163 the worm homolog of mammalian proteasomal trafficking factor ECM29 (LEGGETT *et al.* 2002), *ecps-1,* is
164 depleted, embryos with increased centrosomal SYS-1 were observed, in addition to a second substrate
165 of the centrosomal proteasome, ZYG-1 (PEEL *et al.* 2012; THOMPSON *et al.* 2022). Thus, the current
166 model suggests that SYS-1 and the proteasome are both actively trafficked via dynein to the centrosome
167 during mitosis and, upon proper localization, result in SYS-1 degradation. This model reconciles the
168 observed increase in centrosomal SYS-1 after nocodazole treatment because SYS-1 is more likely to be
169 passively trafficked to the centrosome via diffusion compared to the large proteasome complex. The
170 observed increase in cytoplasmic SYS-1 following RPT-4 knockdown further supports the model in which
171 loss of SYS-1 negative regulation affects its degradation and turnover (THOMPSON *et al.* 2022).
172 While the above model details SYS-1 negative regulation via centrosomal localization during
173 mitosis in the mother cell, SYS-1 is also regulated after an ACD by the β-catenin destruction complex
174 under the regulatory control of WβA in the daughter cells. In response to the Wnt ligand gradient, the
175 WβA pathway polarizes the mother cell and distributes different components of the Wnt-signaling
176 pathway to anterior or posterior poles before mitosis. The positive Wnt regulators, Frizzled and
177 Disheveled, are asymmetrically localized at the posterior cortex, resulting in their enrichment in Wnt-
178 signaled daughter cell after cytokinesis (PARK *et al.* 2004; HARRELL AND GOLDSTEIN 2011; SAWA AND
179 KORSWAGEN 2013; LAM AND PHILLIPS 2017). Negative regulators and members of the destruction
180 complex, APC and Axin, are localized at the anterior pole of the mother cell and are asymmetrically
181 enriched in the anterior Wnt-unsignaled daughter cell. The worm homolog of APC, APR-1, is essential for
182 SYS-1 negative regulation during ACD (ROCHELEAU *et al.* 1997; BARTH *et al.* 2008; BALDWIN AND
183 PHILLIPS 2014). The polar cortical localization of APR-1 is controlled by the worm Axin homolog, PRY-1,
184 which regulates the asymmetry of SYS-1. These data, coupled with the above centrosomal regulation
185 data, suggest the current model of SYS-1 regulation occurs via centrosomal degradation of mother cell
186 SYS-1 and asymmetric regulation of *de novo* synthesized SYS-1 by the destruction complex in the Wnt-
187 signaled and -unsignaled daughter cells (MIZUMOTO AND SAWA 2007; BALDWIN AND PHILLIPS 2014).

188 The current model suggests that centrosomal degradation of mother cell SYS-1 may be complete
189 to prevent inheritance into the daughter cells to ensure proper asymmetric SYS-1 regulation. However,
190 lineage studies show that the Wnt-signaled daughters of Wnt-signaled cells respond more strongly to
191 Wnt signaling in the subsequent division compared to their cousins, the Wnt-signaled daughters of Wnt-
192 unsignaled cells (ZACHARIAS *et al.* 2015; ZACHARIAS AND MURRAY 2016). The heightened response can
193 be visualized by both an enrichment of SYS-1 in the nucleus and increased target gene transcription
194 (ZACHARIAS *et al.* 2015; ZACHARIAS AND MURRAY 2016). This nuclear SYS-1 enrichment suggests SYS-1
195 may be shielded from proteasomal degradation during nuclear localization, allowing for SYS-1
196 inheritance into the daughter cells of previously Wnt-signaled mother cells and progressively enriching
197 the Wnt-signaled lineages for SYS-1 over time. Alternatively, enrichment of positive regulators of SYS-1
198 in Wnt-signaled lineages, such as Frizzled or Dishevelled (SAWA *et al.* 1996; UMBHAUER *et al.* 2000),
199 would also be predicted to increase downstream SYS-1 stabilization. In this latter case, inheritance of
200 upstream Wnt pathway components would be expected to similarly increase WRM-1 and decrease
201 nuclear POP-1 levels between cousins, which was indeed observed in this study (LIN *et al.* 1998;
202 ZACHARIAS *et al.* 2015; ZACHARIAS AND MURRAY 2016). This suggests that increased SYS-1 inheritance
203 from signaled mothers is unlikely to be the sole mechanism of cousin enrichment. However, the extent to
204 which direct SYS-1 inheritance contributes to a Wnt pathway "memory" during normal ACD and how Wnt
205 signaling regulates inherited and *de novo* SYS-1 remains unknown.
206 Here, we show centrosomal degradation of SYS-1 in the EMS mother cell is incomplete, leading
207 to SYS-1 inheritance in the E and the MS daughter cells during wild-type ACDs. We developed a
208 photoconvertible SYS-1 to observe the dynamics of preexisting and newly synthesized SYS-1 at the
209 centrosome during mitosis. We found that preexisting and newly synthesized SYS-1 levels are trafficked
210 to the mitotic centrosome via the dynein complex where they are both degraded. SYS-1 coupling,
211 trafficking, and degradation at the mother cell centrosome are necessary for maintaining sister cell
212 asymmetry and wild-type SYS-1 asymmetry in E and MS daughter cells during ACD. Surprisingly, *de*
213 *novo* SYS-1 increases in both daughter cells after the over-inheritance of mother cell SYS-1 during
214 asymmetric cell division. Additionally, depletion of the negative regulator APR-1 increased both pools of

215 SYS-1 in the E and MS nuclei, suggesting that, when inherited SYS-1 is affected, *de novo* SYS-1 is also
216 misregulated and vice versa. Thus, we propose a model in which SYS-1 centrosomal degradation is a
217 key regulator of SYS-1 inheritance that prevents the loss of daughter cell asymmetry. Further regulation
218 of inherited and *de novo* SYS-1 in the E and MS daughter cells via Wnt signaling supports proper sister
219 cell asymmetry due to a free exchange between the inherited and *de novo* SYS-1 pools.
220

221 Methods

222 Strains

223 Strains were maintained on OP50-inoculated nematode growth media (NGM) plates at 20°C (PHX5708
224 and N2) or 25°C (TX964) using typical *C. elegans* methods (BRENNER 1974). The genotypes of the
225 investigated are as follows: N2 (wild type); TX964 (unc-119(ed3) III; him-3(e1147) IV; teIs98 [$P_{pie-}$
226 $_{1}$::GFP::SYS-1]); BTP254 *(syb5708[*$P_{sys-1::}$DENDRA2::SYS-1*])*.
227

228 CRISPR/Cas9 mediated fluorescent tagging of endogenous SYS-1

229 An in-frame N-terminal DENDRA2-GAS tag was inserted in the endogenous *sys-1* gene prior to the
230 endogenous start codon (SunyBioTech, Fujian, China). Two synonymous nucleotide changes were
231 generated in the donor sequence to prevent the donor from being recognized and cut by Cas9. Genome
232 edited animals were sequence verified with DENDRA-2-*sys-1* specific primers and backcrossed to wild-
233 type N2 worms to reduce the chances of extraneous genetic variation or off target insertions impacting
234 our experiments. The resulting strain, *sys-1(syb5708[*$P_{sys-1::}$DENDRA2::SYS-1*]),* is designated by strain
235 name BTP254.
236

237 RNAi

238 To perform RNAi knockdown of target genes, we used HT115 bacteria containing the pL4440 plasmid
239 with a T7-flanked target gene insert. *rsa-2*, *apr-1* and *ecps-1* were obtained from a library supplied by
240 Ahringer (Addgene) (KAMATH *et al.* 2003). *dlc-1* was obtained from the Phillips lab library and made as
241 described in Thompson *et* al., 2022. Briefly, *dlc-1* was amplified using target gene-flanking primers

242 and *C. elegans* cDNA to generate a new insert. Bacteria with the desired insert were seeded onto
243 isopropyl β-d-1-thiogalactopyranoside (IPTG)-containing plates to induce transcription from the T7
244 promotor as described previously (CONTE *et al.* 2015). Worms were plated onto RNAi bacterial lawns
245 after sodium hypochlorite synchronization as L1s, with the exception of worms plated on *dlc-1* bacterial
246 lawns which were washed from OP50 plates at 24 h before imaging (L3/L4) and plated on to the RNAi
247 plate to avoid larval phenotypes (TIMMONS 2006; BEKAS AND PHILLIPS 2020).
248
249 Confocal microscopy and FRAP
250 Confocal microscopy was performed with a Leica SP8 HyD detector system. The objective used was a
251 63× HC PL APO CS2 objective with N.A. = 1.4, using type F immersion oil. Each analyzed image
252 consisted of 35 summed z-images of the embryo, with each slice approximately 0.6-μm thick. FRAP was
253 performed on the same system. Each embryo was imaged once then photobleached, at anaphase,
254 telophase or cytokinesis. The entire EMS cell was selected as the region of interest (ROI) and bleached
255 at an intermediate focal plane with 100% laser power for 200 iterations. Images were taken immediately
256 after photobleaching at 4, 6, 8 and 10 minutes. Fluorescence intensity was measured on the sum of 6 Z-
257 projection slices in FIJI using the mean fluorescence intensity of ROIs around the nuclei of the E and MS
258 cells.
259
260 Confocal microscopy and photoconversion of DENDRA2::SYS-1
261 Confocal microscopy was performed via a Leica SP8 HyD detector system using a 63× HC PL APO CS2
262 objective with N.A. = 1.4 and type F immersion oil. Each image analyzed consisted of the sum of 35 z-
263 images, approximately 0.6-μm thick, across the embryo. Photoconversion of DENDRA2::SYS-1 was
264 performed on the same system. For centrosome and cytoplasm photoconversion the FRAP software was
265 used to photoconvert the desired locale. Before photoconversion, one image was taken in early
266 metaphase to observe and quantify pre-conversion green SYS-1 levels at the centrosome. The ROI was
267 then photoconverted using the UV laser (405nm diode laser) at an intermediate focal plane with 100%
268 laser power for 200 iterations. Excitation light at 488 nm (490–550 nm) or 552 nm (580–670 nm) was

269 provided by HyD lasers set at 30% laser power for both channels on standard mode. Images were taken
270 immediately after photoconversion every 20 seconds through mitosis of the P1 cell with a frame and line
271 average of 2. To obtain the CEI, the mean intensity of the embryonic cytoplasm was subtracted from the
272 centrosomal mean (THOMPSON *et al.* 2022).
273
274 For whole embryo photoconversion and quantification of DENDRA2::SYS-1 nuclear levels in the E and
275 MS daughter cells, embryos were exposed to a UV laser (405 nm diode laser) at 100% laser power for
276 36 iterations (frame average: 6, line average: 6) using the normal imaging setting on the Leica SP8 HyD
277 detector system. An image was taken of each embryo prior to photoconversion with the excitation light of
278 488 nm (490–550 nm) or 552 nm (580-670) HyD lasers set at 30% laser power for both channels on
279 standard mode. Photoconversion was performed at the time of cytokinesis of the EMS cell, and 2
280 minutes after cytokinesis the timecourse was started, with 1 minute between each image taken for 7
281 minutes. DENDRA2::SYS-1 nuclear levels were normalized by N2 values utilizing the same settings
282 described above.
283
284 Results
285 Photobleaching reveals *de novo* and inherited SYS-1 pools in the E and MS cells and centrosomal SYS-
286 1 dynamics over time.
287 Previous data show changes in centrosomal SYS-1 levels and dynein trafficking correlate with
288 nuclear SYS-1 levels in WβA daughter cells (VORA AND PHILLIPS 2015; THOMPSON *et al.* 2022).
289 Disruption of SYS-1 centrosomal levels by knockdown of the centrosomal scaffold protein RSA-2,
290 different dynein subunits (DHC-1, DLC-1, DYLT-1), or the proteasome trafficking adaptor protein ECPS-1
291 is sufficient to induce a change in cell fate to a Wnt-signaled cell fate in the distal tip cells and the seam
292 cells (THOMPSON *et al.* 2022). These data suggest that impairing SYS-1 centrosomal localization or
293 degradation increases SYS-1 inheritance in the daughters of mother cells that have impaired SYS-1
294 degradation capability. However, it remains possible that degradation of SYS-1 in the mother cell is also
295 incomplete in wild type and that inherited SYS-1 contributes to normal Wnt-dependent asymmetric cell

296 fate specification. To better understand the dynamics of SYS-1 inheritance in wild type, we used
297 fluorescence recovery after photobleaching (FRAP) in the E and MS daughter cells at different time
298 points. The EMS cell is polarized by Wnt ligand produced in the posterior P2 cell, resulting in E and MS
299 daughter cells with high and low nuclear levels of SYS-1, respectively (GOLDSTEIN 1992; HARRELL AND
300 GOLDSTEIN 2011; ROBERTSON AND LIN 2012). The EMS cell was photobleached at different times during
301 mitosis, and the nuclear levels in the E and MS daughter cells were measured (Fig. 1A). Specifically,
302 EMS was photobleached at anaphase, telophase, and cytokinesis and the levels of nuclear SYS-1 in the
303 resulting daughter cells was quantified at four minutes after cytokinesis (Fig. 1B). If SYS-1 is cleared by
304 the mother cell centrosomal processing, we expect no differences between SYS-1 nuclear levels due to
305 EMS photobleaching at different timepoints. Alternatively, if the mother cell SYS-1 protein is inherited by
306 the daughter cells, we expect the largest decrease in SYS-1 levels to occur following the photobleach at
307 cytokinesis. Anaphase photobleach gives slight, non-significant decrease (Fig 1B), but we speculated
308 that this result may be due to SYS-1 synthesis later during mitosis, giving rise to an unbleached
309 population of mother cell SYS-1. To address this, we repeated the photobleaching experiment at
310 telophase and at cytokinesis. Indeed, after the EMS telophase photobleach, we observed significant
311 decreases in E and MS nuclear SYS-1, suggesting the degradation of SYS-1 is incomplete in the mother
312 EMS cell (Fig. 1B, S1). Finally, due to the possibility of late cell cycle SYS-1 synthesis, we
313 photobleached at cytokinesis to rule out mother cell contribution to daughter cell signal. Despite the late
314 timing of the photobleaching, GFP::SYS-1 was still visible in both daughter cell nuclei, revealing both a
315 mother cell contribution and a *de novo* synthesized SYS-1 pool in the E and the MS daughter cells (Fig.
316 1B). Regardless of the time of photobleaching, the asymmetry between E and MS SYS-1 nuclear levels
317 is maintained (Fig. 1B). These results suggest SYS-1 mother cell clearance is incomplete and that *de*
318 *novo* SYS-1 is asymmetrically regulated during EMS ACD.

319 To observe the dynamics of the *de novo* SYS-1 pool in the daughter cells, we photobleached the
320 EMS mother cell at cytokinesis and measured *de novo* and total nuclear SYS-1 at different times (4, 6, 8,
321 and 10 mins after cytokinesis) (Fig. 1C). We measured SYS-1 levels of the E and MS cells at different
322 times with and without photobleaching at cytokinesis to determine the effect of the EMS cell cycle on

323 total and *de novo* SYS-1 accumulation over time. Because *de novo* nuclear SYS-1 levels were reduced
324 by 45–83% relative to total SYS-1 levels at each time point, our results suggest SYS-1 inheritance
325 occurs in wild type from the EMS into the E and MS daughter cells and that photobleaching at
326 cytokinesis has a measurable effect on SYS-1 levels throughout the daughter cell cycle.

327 Interestingly, the accumulation of *de novo* SYS-1 was not linear. Instead, we observed a
328 significant increase in nuclear *de novo* SYS-1 levels in both daughter cells during minutes four through
329 six, as expected given the time needed for new synthesis (Fig. 1D). However, *de novo* SYS-1 levels
330 plateau around 8 min and then decrease at 10 min, after cytokinesis of the mother cell (Fig. 1D),
331 suggesting *de novo* SYS-1 accumulation changes throughout the cell cycle. To quantify this change, we
332 calculated the ratio of total to *de novo* nuclear SYS-1 levels over the timecourse in both daughter cells. In
333 the E cell at four minutes, the *de novo* SYS-1 pool represents about one-third (Fig. 1E, 4 min=28.9%) of
334 the total SYS levels and increases to roughly half (6 min=54.2%; 8 min=51.5%) by minutes 6–8 after
335 mother cell division. Ten minutes after cytokinesis *de novo* SYS-1 decreases to 33%. We observe a
336 similar pattern in the MS cell (4 min=17%; 6 min=45%; 8 min=50%; 10 min=29%), though the absolute
337 levels are higher in the Wnt-signaled E daughter (Fig. 1D). This timecourse revealed variable rates of *de*
338 *novo* SYS-1 synthesis and regulation in the nuclei of the E and MS daughter cells through the cell cycle,
339 suggesting the role of Wnt signaling in SYS-1 stabilization is mostly complete by 8 minutes post-EMS
340 division and, surprisingly, that the "unsignaled" MS cell also stabilizes SYS-1, albeit at a lower level than
341 E.

342 <u>Photoconversion of DENDRA2::SYS-1 reveals turnover at the centrosome during mitosis.</u>

343 To visualize *de novo* and inherited SYS-1, we generated a photoconvertible *sys-1* transgene,
344 $P_{sys-1}$::DENDRA2::SYS-1. With this new tool, we were able to observe and differentiate preexisting (red)
345 and newly synthesized (green) SYS-1 centrosomal accumulation in the P1 cell, which has been
346 previously utilized for SYS-1 centrosomal localization and processing studies (VORA AND PHILLIPS 2015;
347 THOMPSON *et al.* 2022). While observing P1 cellular division, in the green channel DENDRA2::SYS-1 is
348 visible at the centrosome prior to photoconversion, consistent with previous studies (VORA AND PHILLIPS
349 2015; THOMPSON *et al.* 2022) (Fig. 2A), while the red channel detection shows a lack of DENDRA2::SYS-

350 1 at the centrosomes (Fig. 2B). To photoconvert DENDRA2::SYS-1 from green to red fluorescence, we
351 exposed the entire P1 cell to a UV laser (405nm diode laser) (CHUDAKOV *et al.* 2007) at 100% laser
352 power for 36 iterations. After photoconversion, centrosomal DENDRA2::SYS-1 in the green channel
353 sharply decreases (Fig. 2C) and we clearly detect red fluorescent DENDRA2::SYS-1 at the centrosome
354 (Fig. 2D). After confirming successful photoconversion, we measured centrosomal DENDRA2::SYS-1
355 levels in 20-second increments through P1 mitosis (Fig. 2E). In order to control possible photoconversion
356 by the 488nm laser (WOODS *et al.* 2014), we followed the same imaging protocol without 405nm
357 photoconversion and followed both emissions over the timecourse. The data were normalized using N2
358 animals subjected to the same protocol to account for possible photobleaching or changes in
359 development of the embryo induced by the imaging. Our data shows that there is no photoconversion
360 induced by repetitive imaging with the 488nm laser as no changes are observed in the red channel (Fig.
361 S2A). The raw data revealed the preexisting, red centrosomal DENDRA2::SYS-1 decreased over time,
362 likely due to centrosomal degradation. Interestingly, the newly synthesized, green centrosomal
363 DENDRA2::SYS-1 decreased at a slower rate throughout the rest of P1 mitosis (Fig. 2F). Additionally, to
364 quantify photoconversion efficacy, we compared the level of post-conversion red signal to the green
365 signal after mock conversion, both normalized for green pre-conversion signal (Fig. S2A, B). The results
366 indicate ratios of approximately one and no significant difference between the two ratios, indicating
367 successful photoconversion. Together these data suggest that the rate of synthesis and trafficking is
368 relatively equal to the rate of degradation of *de novo* SYS-1 at the centrosome, which is consistent with
369 the previously published idea of a steady-state level of centrosomal GFP::SYS-1 that is stable during the
370 P1 cell mitosis (Vora and Phillips, 2015).

371 To specifically evaluate the enrichment of DENDRA2::SYS-1 at the centrosome, we used the
372 centrosomal enrichment index (CEI) (THOMPSON *et al.* 2022). The CEI allows us to measure the degree
373 to which the mother cell traffics cytoplasmic SYS-1 to the centrosome, thus enriching SYS-1
374 fluorescence at the centrosome, while also internally controlling for bleaching via repetitive imaging. The
375 CEI measurement allowed us to more clearly observe the initial increase in the red channel of
376 centrosomal DENDRA2::SYS-1 after photoconversion (Fig. 2G). The CEI data show a similar rate of

377 declining preexisting DENDRA2::SYS-1 centrosomal levels as the raw data but emphasizes the stability
378 of newly translated centrosomal DENDRA2::SYS-1 enrichment, which is stable and low (Fig. 2G). Since
379 we would expect no centrosomal enrichment of preexisting DENDRA2::SYS-1 if SYS-1 were trafficked to
380 a different locale to be degraded, our finding that older SYS-1 preferentially localizes to the centrosomes
381 is consistent with our model of SYS-1 enrichment from the cytoplasm and subsequent degradation at the
382 centrosome.
383 Altogether, these data suggest that newly synthesized and trafficked SYS-1 coupled with degradation of
384 preexisting centrosomal SYS-1 lead to a stable steady state at the centrosomal locale, while indicating
385 that the centrosome is the terminal locale of SYS-1. Notably, degradation is sequential as pre-existing
386 SYS-1 at the centrosome is degraded prior to the newly trafficked SYS-1 which is stably replenished by
387 cytoplasmic trafficking dependent on dynein.
388 <u>Photoconversion of the cytoplasm of the P1 cell unveils dynamics of dynein trafficking of</u>
389 <u>DENDRA2::SYS-1 during mitosis.</u>
390 Previous data showed that microtubule trafficking via the dynein complex is needed for SYS-1
391 centrosomal localization (THOMPSON *et al.* 2022). By photoconverting subdomains of the posterior pole of
392 the P1 cell cytoplasm, we tested the ability of the cell to traffic SYS-1 to the centrosomes. Following initial
393 imaging during early mitosis, where pre-conversion levels of centrosomal DENDRA2::SYS-1 were
394 measured with both green and red emission, a portion of the cytoplasm was photoconverted (Fig. 3A).
395 After photoconversion, embryos were imaged every 20 seconds during mitosis (Fig. 3B). After
396 photoconversion of the cytoplasm, DENDRA2::SYS-1 levels were measured in the proximal and the
397 distal centrosomes (Fig. 3A), in both the green and red channels. The photoconverted, red
398 DENDRA2::SYS-1 represents newly trafficked SYS-1 from the posterior cytoplasmic region of the
399 embryo, while green DENDRA2::SYS-1 denotes older pre-existing centrosomal SYS-1 and newly
400 trafficked SYS-1 from the non-photoconverted cytoplasmic SYS-1. Quantification of red newly trafficked
401 SYS-1 showed centrosomal localization in both the proximal and distal centrosomes 20 seconds after
402 photoconversion (Fig.3C, 3D), suggesting that SYS-1 is highly mobile and quickly trafficked to both
403 centrosomes in early mitosis. However, though photoconverted SYS-1 accumulates on both proximal

404 and distal centrosomes, the rates of accumulation are not equal. In the green channel, both the proximal
405 and the distal centrosomes exhibit similar DENDRA2::SYS-1 levels, and both show an initial small
406 increase followed by a steady decline (Fig. 3C). These data suggest that trafficking occurs in early
407 mitosis to both centrosomes, in which rates of trafficking and degradation of DENDRA2::SYS-1 are
408 similar, consistent with prior observations (VORA AND PHILLIPS 2015; THOMPSON *et al.* 2022). When
409 directly comparing newly trafficked DENDRA2::SYS-1 levels in the proximal and distal centrosomes, we
410 observe that proximal centrosomes have a higher enrichment of SYS-1 throughout mitosis when
411 compared to distal centrosomes (Fig. 3D). The difference in centrosomal DENDRA2::SYS-1 levels
412 between the centrosomes suggest that cytoplasmic SYS-1 from any locale can be trafficked to both
413 centrosomes but is more likely to be trapped and trafficked via dynein to the most proximal centrosome.
414 To observe the impact of microtubule trafficking on DENDRA2::SYS-1, we knocked down the light
415 subunit of the dynein complex, DLC-1, via RNAi feeding and measured the CEI of photoconverted
416 DENDRA2::SYS-1 in the proximal centrosome. Previous results show DLC-1 is required for efficient
417 centrosomal enrichment of SYS-1 (THOMPSON *et al.* 2022). After *dlc-1(RNAi),* the red, newly trafficked
418 DENDRA2::SYS-1 is stable throughout mitosis; however, DLC-1 knockdown hinders SYS-1 trafficking to
419 the centrosome, resulting in a decrease of centrosomal SYS-1 enrichment throughout mitosis compared
420 to controls (Fig. 3E). This result is consistent with impaired SYS-1 centrosomal recruitment observed in
421 cells lacking efficient dynein trafficking (THOMPSON *et al.* 2022). These data, which is consistent with our
422 model of SYS-1 capture and centrosomal trafficking, suggest microtubule trafficking via the dynein
423 complex is key for centrosomal SYS-1 localization and subsequent degradation.
424
425 <u>E and MS inheritance of mother cell SYS-1 is limited by EMS centrosomal processing.</u>
426 To determine the extent to which changes in SYS-1 centrosomal trafficking and degradation
427 affect inheritance of mother cell SYS-1 into the daughter cells, we photoconverted the entire EMS cell of
428 DENDRA-2::SYS-1-expressing embryos at cytokinesis and measured inherited (red) SYS-1 in the E and
429 MS daughter cell nuclei. As the first ACD driven by the Wnt/β-catenin asymmetry pathway, we
430 specifically analyzed the EMS cell division (HARRELL AND GOLDSTEIN 2011). Here, the E cell is the Wnt-

431 signaled cell that normally exhibits higher SYS-1 levels, and the MS daughter is the unsignaled cell with
432 lower SYS-1 levels (HUANG *et al.* 2007; PHILLIPS *et al.* 2007). For photoconversion of DENDRA2::SYS-1,
433 we exposed the whole EMS cell to a UV laser (405nm diode laser) (CHUDAKOV *et al.* 2007) at 100% laser
434 power for 36 iterations during cytokinesis of the EMS cell. Subsequently, we waited two minutes for the
435 nuclear envelope of the E and MS daughters to reform and imaged every 60 seconds for 7 minutes (Fig.
436 4A). Then, we normalized the nuclear fluorescence of DENDRA2::SYS-1 to the nuclear autofluorescence
437 in wild-type (N2) embryos using identical measurements. Consistent with our FRAP studies, we
438 observed inherited DENDRA2::SYS-1 present in into both E and MS daughter cells (Fig. 4B).
439 Interestingly, the amount of DENDRA2::SYS-1 inherited by the E daughter was higher than that inherited
440 by the MS cell (Fig. 4B), perhaps reflecting greater stability of inherited SYS-1 in the signaled E cell. We
441 also noted that MS inheritance, while lower than E, was on average above autofluorescence. This result
442 indicates SYS-1 inheritance persists even in the unsignaled MS cell. The timecourse also allowed us to
443 observe changes in nuclear DENDRA2::SYS-1 over the cell cycle of the E and MS cells, up to 9 minutes
444 after EMS division. For both the E and MS daughter cells, we found inherited nuclear DENDRA2::SYS-1
445 levels to remain stable throughout the timecourse (Fig. 4B). This result indicates the asymmetry in
446 inherited nuclear DENDRA2::SYS-1 occurs shortly after EMS division.

447 Next, we tested the requirement for dynein trafficking and centrosomal localization in SYS-1
448 inheritance. We predicted that impaired mother cell SYS-1 processing would lead to an increase in
449 inherited SYS-1 levels, given the previously observed changes in cell fate under these conditions (DLC-
450 1, RSA-2 and ECPS-1 knockdowns) (THOMPSON *et al.* 2022). We observed that when microtubule
451 trafficking is impaired by the knockdown of DLC-1 there is a significant increase in the amount of
452 inherited DENDRA2::SYS-1 nuclear levels of both the E and MS cells (Fig. 4C). Initial levels of inherited
453 SYS-1 were 3 and 10-fold higher in the E and MS cells, respectively (Fig. 4C). These data suggest
454 mother cell dynein trafficking is required to limit the amount of inherited SYS-1.

455 We further investigated the role of SYS-1 centrosomal localization in controlling SYS-1
456 inheritance by preventing centrosomal localization of SYS-1 via knockdown of the centrosomal scaffold
457 protein RSA-2. RSA-2 provides a necessary centrosomal scaffold and acts as a direct binding partner for

458 SYS-1 localization at the mitotic centrosome (VORA AND PHILLIPS 2015). Loss of centrosomal localization
459 by *rsa-2(RNAi)* increased the amount of inherited nuclear DENDRA2::SYS-1 by 3.4- and 11-fold in E and
460 MS daughter cells, respectively (Fig. 4D). Lastly, we impaired the degradation of centrosomal SYS-1 by
461 knocking down the adaptor protein ECPS-1, the worm homolog to EMC29, (a proteasome-dynein
462 adaptor and scaffold (LEGGETT *et al.* 2002; LEHMANN *et al.* 2010). Previous studies showed that ECPS-1
463 knockdown leads to an increase of SYS-1 levels at the centrosome, suggesting its role in SYS-1
464 centrosomal degradation (THOMPSON *et al.* 2022). *ecps-1*(RNAi) lead to an increase of the amount of
465 DENDRA2::SYS-1 inherited into the E and MS cells by 3- and 10.7-fold, respectively (Fig. 4E). These
466 data suggest that ECPS-1 knockdown impairs degradation of SYS-1 in the centrosome of the mother cell
467 and that ECPS-1 function is normally required to prevent SYS-1 over-inheritance.
468 Finally, to assess the effect of the over-inherited SYS-1 on loss of daughter cell SYS-1
469 asymmetry and further loss of the asymmetric cell division of EMS, we averaged the inherited
470 DENDRA2::SYS-1 nuclear levels in each condition throughout the 7-minute timecourse and measured
471 the fold change between the E and the MS daughters. These data showed a loss of asymmetry of
472 inherited SYS-1 in all the experimental conditions tested compared to control RNAi (Fig. 4F). The data
473 suggest that, in wild-type conditions, SYS-1 is inherited into both the E and the MS daughter cells, and
474 that early in the cell cycle, the asymmetry between E and MS is established. For proper inheritance of
475 SYS-1 during the EMS ACD the mother cell requires SYS-1 centrosomal trafficking, coupling, and
476 degradation (also referred to as centrosomal processing) to prevent over-inheritance of SYS-1 and loss
477 of sister cell asymmetry, seen by a reduction in the P:A ratio after loss of centrosomal SYS-1 processing
478 (Fig 4F).
479
480 <u>Loss of centrosomal SYS-1 results in increased levels of nuclear *de novo* SYS-1 in EMS daughter cells.</u>
481 Previously, we showed that loss of trafficking, centrosomal coupling or degradation of SYS-1
482 leads to higher SYS-1 levels in the daughter cells (Fig. 4) (VORA AND PHILLIPS 2015; THOMPSON *et al.*
483 2022), which can in turn lead to a loss off the asymmetric cell division (THOMPSON *et al.* 2022). Given the
484 fact that centrosomal processing functions in the mother cell to control over inheritance, we predicted

485 that mother cell, but not *de novo* translated DENDRA2::SYS-1 would be affected when mother cell
486 centrosomal processing of SYS-1 is impaired. To test this, we first measured green/*de novo*
487 DENDRA2::SYS-1 nuclear levels in the E and MS daughter cell over time starting 2 minutes after
488 cytokinesis and in 60 second increments for 7 minutes (Fig. 5A, B). We observed that both the E cell, the
489 Wnt-signaled cell, and MS, the unsignaled cell, were actively translating DENDRA2::SYS-1 (Fig. 5A),
490 consistent with our FRAP results (Fig.1C). The E cell also showed higher levels of *de novo* nuclear
491 DENDRA2::SYS-1 levels than the MS cell (3.6-fold increase in E vs MS), indicating robust asymmetry in
492 synthesis or stability of newly translated DENDRA2::SYS-1 (Fig. 5B). Additionally, the timecourse
493 showed that the E and MS *de novo* nuclear DENDRA2::SYS-1 levels remained stable (Fig. 5B). These
494 data suggest that SYS-1 synthesis occurs in both the signaled E and unsignaled MS daughter cells and
495 that the synthesis/maintenance rates are higher in E than MS.
496 Subsequently, we observed *de novo* nuclear DENDRA2::SYS-1 levels in the daughter cells after
497 knocking down DLC-1, therefore impairing microtubule trafficking of SYS-1 to the centrosome in the
498 mother cell (THOMPSON *et al.* 2022). This surprisingly resulted in a significant increase in the amount of
499 *de novo* nuclear SYS-1 levels in both daughter cells at all time points (Fig. 5C). This increase in *de novo*
500 SYS-1 was also observed in the other tested conditions that showed increased DENDRA2::SYS-1
501 inheritance, *rsa-2* and *ecps-1 (*RNAi) (Fig. 5D,E). In all the tested conditions (*dlc-1, rsa-2* and *ecps-1*
502 *(*RNAi)), we also observed a loss of asymmetry compared to the control (Fig. 5F).
503 Thus, we find that impairing proper SYS-1 centrosomal processing during mitosis of the EMS cell
504 showed increased levels of both inherited and *de novo* nuclear DENDRA2::SYS-1 in EMS daughter cells
505 (Fig. 4C, D, E and Fig. 5C, D, E). Additionally, we observed that over time in the tested conditions,
506 nuclear DENDRA2::SYS-1 consistently decreases in backgrounds with higher than normal SYS-1
507 compared to wild type, which stably maintains its SYS-1 levels in E and MS (Fig. 4C, D, E and Fig. 5C,
508 D, E) (Table 1). This pattern of increased rate of DENDRA2::SYS-1 loss was observed in both
509 DENDRA2::SYS-1 pools, suggesting that both pools, *de novo* and inherited, in the E and MS cells are
510 processed similarly. These data suggest that over-inheritance of SYS-1 during asymmetric cell division
511 affects the *de novo* SYS-1 that is generated or maintained in both daughter cells. This led us to

512 hypothesize that the β-catenin "destruction complex" activity in daughter cells has a limited capacity and
513 is not fully able to regulate SYS-1 properly in situations with increased levels of inherited SYS-1, an idea
514 we test below.
515
516 Partial loss of the negative regulator of the Wnt signaling pathway, APR-1, affects both pools of nuclear
517 SYS-1 in the E and MS cells.
518 To investigate the role of the destruction complex in regulating *de novo* and inherited SYS-1
519 during asymmetric cell division and during the cell cycle of the E and MS daughter cells we impaired a
520 SYS-1 negative regulator of the Wnt pathway, APR-1 (HUANG *et al.* 2007; BALDWIN AND PHILLIPS 2014).
521 APR-1 is a homolog of vertebrate APC, which is part of the β-catenin destruction complex and functions
522 to limit β-catenin cytoplasmic accumulation in the Wnt-unsignaled state. APC/APR-1 also limits Wnt
523 pathway activity after initial activation by targeting β-catenin for proteasomal degradation (CLEVERS AND
524 NUSSE 2012). As expected, we found that partial depletion of APR-1 via RNAi feeding led to a significant
525 increase in *de novo* DENDRA2::SYS-1 nuclear levels throughout the MS cell cycle (Fig. 6A). We also
526 observed a 2-fold increase in *de novo* DENDRA2::SYS-1 during the E cell cycle (Fig. 6A), which has not
527 been shown previously. This result was unexpected as a role of APR-1 as a negative regulator of SYS-1
528 had been primarily observed in the unsignaled MS cell (HUANG *et al.* 2007; SUGIOKA *et al.* 2011; BALDWIN
529 AND PHILLIPS 2014; BALDWIN *et al.* 2016), while these data suggest APR-1 regulates SYS-1 levels in both
530 daughter cells.
531 Additionally, we observe different nuclear DENDRA2::SYS-1 dynamics when APR-1 is knocked
532 down compared to other backgrounds with elevated *de novo* DENDRA2::SYS-1. The E and MS cells *de*
533 *novo* DENDRA2::SYS-1 levels show a smaller decrease compared to the DLC-1, RSA-2, and ECPS-1
534 knockdowns (Table 1), over the 7-minute timecourse (Fig. 6A). These results suggest that *de novo* SYS-
535 1 in both daughter cells is limited by the destruction complex in wild type and in situations with elevated
536 inherited SYS-1.
537 We observed increased levels of inherited nuclear SYS-1 in both E and MS daughter cells after
538 APR-1 depletion (Fig. 6B). The role of APR-1 in negative SYS-1 regulation in the signaled E cell was

539 surprising due to previous observations that demonstrate higher APR-1 levels in the MS cell and that
540 APR-1 depletion primarily affects MS specification rather than E (HUANG *et al.* 2007; SUGIOKA *et al.*
541 2011). We proceeded to quantify the changes in inherited DENDRA2::SYS-1 nuclear levels in the E and
542 MS on *apr-1(*RNAi), to observe the effect that APR-1 knockdown directly has on the inherited SYS-1
543 pool. We observed the highest fold change of *de novo* nuclear DENDRA2::SYS-1 in *apr-1(RNAi)* in the
544 MS cell compared to wild type (Fig. 6C). In MS, the *de novo* pool was more highly affected by loss of
545 APR-1 than the inherited pool, suggesting that, in wild type, APR-1 more highly negatively regulates *de*
546 *novo* DENDRA2::SYS-1 in the MS cell (Fig. 6C). Though the effect of APR-1 depletion on inherited SYS-
547 1 in MS leads to an average of 3.1-fold increase compared to wild type; this was less than the 7.9-fold
548 increase we see in the MS *de novo* SYS-1 pool. By contrast, the difference between E inherited and E *de*
549 *novo* SYS-1 after APR-1 depletion is not as striking (1.4-fold and 2.3-fold increase compared to wild type,
550 respectively) (Fig. 6C).

551 Overall, while we do see an effect of APR-1 regulation of SYS-1 in the E daughter cell, the fold
552 change of DENDRA2::SYS-1 nuclear *de novo* levels is not as drastic in E compared to MS, where we
553 observe a nearly 8-fold increase in the newly translated SYS-1 on *apr-1(*RNAi) (Fig. 6C). Therefore, the
554 major regulatory function of APR-1 on SYS-1 nuclear levels in EMS ACD is to limit accumulation of *de*
555 *novo* SYS-1 in MS. In the E cell, APR-1 plays a minor role SYS-1 regulation, likely due to APR-1
556 repression due to Wnt signaling.

557 Despite the decreased effect of APR-1 depletion on DENDRA2::SYS-1 nuclear levels in E, our
558 results suggest that APR-1 is also functioning in this Wnt-signaled daughter cell. However, an alternative
559 hypothesis explaining our increased SYS-1 levels in E after APR-1 depletion is that APR-1 negatively
560 regulates SYS-1 earlier in the EMS lineage. In this case, increased SYS-1 inheritance is would be
561 expected to increase the total SYS-1 levels and possibly the stability of *de novo* SYS-1 in the daughter
562 cells. To distinguish between these possibilities, we knocked down APR-1 and observed changes in total
563 centrosomal DENDRA2::SYS-1 levels in the EMS cell during mitosis with no photoconversion.
564 Centrosomal SYS-1 quantitation is a good readout of SYS-1 levels in the EMS cell and its progenitors
565 because SYS-1 centrosomal accumulation reflects cytoplasmic SYS-1 levels (VORA AND PHILLIPS 2015)

566 and any effect of SYS-1 levels can be clearly observed immediately before the cell divides, providing the
567 latest timepoint possible before the birth of E and MS. We found that there is no significant change in
568 centrosomal DENDRA2::SYS-1 levels during telophase of the EMS cell on *apr-1(RNAi)* compared to wild
569 type (Fig. 6D), suggesting SYS-1 is not negatively regulated by APR-1 in EMS or its progenitors. Thus,
570 our observations suggest that when the inherited SYS-1 pool is affected in the EMS mother cell, the *de*
571 *novo* SYS-1 pools are secondarily affected in the daughter cells. Additionally, here we observed a role
572 for APR-1 limiting the accumulation of both SYS-1 pools in both the signaled and unsignaled EMS
573 daughter cells.
574
575 Discussion
576 In *C. elegans,* successful asymmetric cell divisions throughout development depend on proper
577 regulation of SYS-1 levels. Here we show that in wild-type conditions, proper SYS-1 centrosomal
578 degradation in the EMS mother cell is key to regulate inheritance into the E and MS cells during ACD. It
579 was previously established that SYS-1 centrosomal trafficking, coupling and degradation in the mother
580 cell is key for regulation of limiting subsequent daughter cell SYS-1 levels and subsequent asymmetric
581 cell fate specification (VORA AND PHILLIPS 2015; THOMPSON *et al.* 2022). These data suggested SYS-1
582 inheritance was normally limited by centrosomal degradation and that *de novo* synthesized SYS-1,
583 regulated by asymmetric Wnt pathway activity, was the source of nuclear SYS-1 important for ACD.
584 However, SYS-1 inheritance (or the lack thereof) and the role of centrosomal degradation have not been
585 demonstrated. Photobleaching experiments show that mother cell bleaching of GFP::SYS-1 decreases
586 the total GFP::SYS-1 in the daughter cells, suggesting that inherited SYS-1 was present in daughter cell
587 nuclei in wild-type conditions. DENDRA2::SYS-1 photoconversion at cytokinesis directly confirmed
588 DENDRA2::SYS-1 inheritance to both the E and the MS cell and that loss of centrosomal SYS-1
589 degradation not only increases the inherited DENDRA2::SYS-1 pool but also unexpectedly
590 increases/stabilizes the *de novo* synthesized pool. We show that APR-1 regulates both inherited and *de*
591 *novo* SYS-1 in E and MS, and the rate of clearance of extra inherited SYS-1 is dependent on APR-1
592 function. Photoconvertible SYS-1 also allowed us to test the model of SYS-1 trafficking to its final

593 destination in the cell, the mitotic centrosome. Photoconversion of DENDRA2::SYS-1 at the centrosome
594 during metaphase demonstrated that newly synthesized DENDRA2::SYS-1 is continually trafficked to the
595 centrosome during mitosis, resulting in stable steady state SYS-1 levels despite this localization leading
596 to increased SYS-1 turnover (VORA AND PHILLIPS 2015). In contrast, preexisting SYS-1 is more enriched
597 at the centrosome and decreases through mitosis. Thus, proper SYS-1 levels are dependent on both
598 trafficking and degradation of SYS-1 in the mother cell along with negative regulation via the destruction
599 complex in the daughter cells.

600 Based on our findings, we proposed the following model (Fig. 7):

601 In wild-type conditions during ACD of the EMS cell, a portion of cytoplasmic SYS-1 is trafficked to
602 the centrosome via the dynein complex where the scaffold protein RSA-2 allows for SYS-1 to localize to
603 the centrosome. Centrosomal SYS-1 is degraded by the centrosomal proteosome, while the remaining
604 cytoplasmic SYS-1 is inherited into the E and MS daughter cells. Inherited SYS-1 is then differentially
605 regulated by APR-1, primarily (but not exclusively) in MS cell. *De novo* SYS-1 also accumulates in both
606 daughter cells, with the E cell having higher nuclear SYS-1 levels than the MS cell, and the *de novo* pool
607 is similarly regulated by APR-1 as the inherited pool (Fig. 7A).

608 Loss of mother cell regulation of centrosomal SYS-1 levels via depletion of RSA-2, DLC-1 or
609 ECPS-1 prevents proper degradation of mother cell SYS-1 leading to over-inheritance of SYS-1 in both
610 daughter cells. A higher rate of SYS-1 inheritance is correlated with higher *de novo* SYS-1 levels in both
611 daughter cells, indicating an inability of the destruction complex to effectively regulate both SYS-1 pools
612 due to dilution of the destruction complex activity. The overwhelming of the destruction complex allows
613 SYS-1 nuclear levels to be higher in both the E and MS cell (Fig. 7B).

614 Loss of the negative regulator APR-1 has a direct effect in the *de novo* levels in both the E and
615 the MS cells as we see no effect on EMS mother cell SYS-1 levels (Fig. 6D). Due to the similar
616 regulation of *de novo* SYS-1 and inherited SYS-1 pools by APR-1, increased levels of both pools were
617 observed after APR-1 depletion, however this was likely due to increased stability of just the *de novo*
618 pool. A loss of APR-1 therefore leads to increased total SYS-1 levels and a loss of daughter cell
619 asymmetry (Fig. 7C) (HUANG *et al.* 2007).

620 Focusing on at the EMS cell during cytokinesis, our model proposes that the polarization of the
621 cell via the Wnt gradient leads to differential distribution of APR-1. In the posterior region of the mother
622 cell, APR-1 will not accumulate due to increased Wnt signaling (Fig. 7D). In the anterior region of the cell,
623 as documented previously (SUGIOKA *et al.* 2018), there will be a greater accumulation of APR-1. This
624 pattern of APR-1 asymmetry will drive asymmetric stability of SYS-1 post division (Fig. 7E,F). In the first
625 portion of the daughter cell cycle, from two to six minutes post-cytokinesis (Fig 7E), the E cell increases
626 its total nuclear SYS-1 levels, which encompasses the inherited and the *de novo* SYS-1 pools, due to
627 decreased APR-1 levels and activity resulting from active Wnt signaling. During this same period of time,
628 APR-1 in the MS cell decreases SYS-1 stability, leading to low total nuclear SYS-1 levels. Late during
629 the cell cycle of the daughter cells, eight to ten minutes after cytokinesis (Fig. 7F), we observe decreased
630 total SYS-1 levels in the E cell due to increasing negative regulation via APR-1. In the MS cell, a more
631 pronounced SYS-1 decrease is observed, suggesting a lack of Wnt signaling and the negative regulation
632 of *de novo* and inherited SYS-1 via APR-1 (Fig. 7F).
633
634 <u>Why do we observe differential levels of inherited SYS-1?</u>
635 Here we conduct the first examination of SYS-1 inheritance during ACD to test the ability of
636 mother cells to regulate the level of SYS-1 in its daughters. A photoconvertible DENDRA2::SYS-1 under
637 the endogenous promoter enabled the observation and quantification of DENDRA2::SYS-1 inheritance
638 during the ACD of the EMS cell (Fig. 4B). Interestingly, the inherited DENDRA2::SYS-1 is not equal for
639 both daughter cells, E shows higher levels of SYS-1 through the timecourse than its sister MS (Fig. 4A).
640 Previous studies show a strong asymmetry of APR-1 during the EMS cell division, accumulating in the
641 anterior side (SUGIOKA *et al.* 2011; SUGIOKA *et al.* 2018). Our data showed that APR-1 predominantly
642 functions in the MS cell, though we do also see APR-1 depletion effects in E (Fig. 6C). This suggests that
643 SYS-1 inheritance may be symmetric (VORA AND PHILLIPS 2015), or at least correlates with the volume of
644 the cytoplasm, but the stability of SYS-1 is asymmetric in the two daughter cells. In this model, inherited
645 DENDRA2::SYS-1 in wild type condition is more stable and prevalent in the E cell (Fig. 4B). However, it
646 remains feasible that asymmetric inheritance of other Wnt signaling components, such as Frizzled or

647 Dishevelled, contribute to the asymmetry observed. Indeed, asymmetric MOM-5/Frizzled has been
648 reported in the early embryonic blastomeres (PARK *et al.* 2004) and the seam cells (MIZUMOTO AND SAWA
649 2007), suggesting these components could be influencing the distribution of other Wnt signaling
650 components during ACD. All together, these data suggest that while SYS-1 might be symmetrically
651 inherited into the daughter cells, further SYS-1 regulation and stability is dependent on the asymmetric
652 inheritance of positive and negative regulators of Wnt-signaling.
653
654 Why does over-inheritance of SYS-1 correlate with higher *de novo* SYS-1 levels?
655 While loss of microtubule trafficking, centrosomal coupling or degradation of SYS-1 in the mother
656 cell led to an increase in the amount of inherited DENDRA2::SYS-1, we also observed increased levels
657 of *de novo* DENDRA-2::SYS-1 in both daughter cells. These unexpected results led to further
658 investigation of the role of negative regulators of SYS-1 in the Wnt-signaling pathway. Since APR-1
659 depletion primarily affects *de novo* DENDRA2::SYS-1 rather than DENDRA2::SYS-1 levels in the mother
660 cell (Fig 6A, D), we used this background to test the effect of increased *de novo* DENDRA2::SYS-1 on
661 maintenance of the inherited DENDRA2::SYS-1 pool. We observed increased inherited nuclear
662 DENDRA2::SYS-1 levels in both daughter cells (Fig. 6B). These results supported our hypothesis that
663 when either of the pools is affected, this will influence the amount of nuclear SYS-1 in the other pool.
664 These results could be explained by an overwhelming of the destruction complex that is equally targeting
665 both *de novo* and inherited SYS-1 pools, thus leading to an accumulation of *de novo* SYS-1 as
666 destruction complex activity is diluted by increased inherited SYS-1. Our data suggest that increased
667 levels of SYS-1 in the daughter cells directly increases SYS-1 stability in the primarily affected pool
668 (inherited DENDRA2::SYS-1 in *dlc-1, rsa-2 and ecps-1*(RNAi) or *de novo* DENDRA2::SYS-1 in *apr-*
669 *1*(RNAi)), which in turn perturbs negative regulation of the other pool, leading to an increase in the total
670 levels of nuclear SYS-1. Thus, we conclude that the SYS-1 pools are interchangeable, and both
671 regulated by the destruction complex.
672 APR-1 depletion also allowed to test the hypothesis that the rate of nuclear SYS-1 loss observed
673 where we have high levels of inherited DENDRA2::SYS-1 (RSA-2, ECPS-1, or DLC-1 depletion) are due

674 to the function of the destruction complex degradation of SYS-1 back to basal levels. APR-1 knockdown,
675 though causing elevated SYS-1 levels, also led to a more moderate rate of decrease in *de novo* SYS-1
676 levels throughout the timecourse compared to the other conditions tested (*dlc-1, rsa-2 and ecps-*
677 *1(RNAi)*), suggesting efficient clearance of extra SYS-1 requires APR-1 (Table1) (Fig. 6A). However,
678 when we observed inherited DENDRA2::SYS-1 on *apr-1* (RNAi) levels still decreased over time. Whether
679 this is due to inherent instability of SYS-1 protein, insufficient knockdown of APR-1 or another SYS-1
680 degradation mechanism remains elusive.
681
682 <u>APR-1 functions in the E cell?</u>
683 Our data suggest that the destruction complex functions in the Wnt-signaled E cell. When
684 knocking down APR-1, we found increased levels of *de novo* nuclear DENDRA2::SYS-1 in both the E
685 and the MS, and while this result was expected for the MS cell, we did not expect to see significant
686 changes in the E cell (Fig. 6A and B). Previous studies investigated the kinetic responses of β-catenin to
687 Wnt-signaling in mammalian cells and found that the destruction complex functions in both the absence
688 and presence of Wnt-signaling. However, when Wnt ligand is present, the destruction complex is only
689 partially active (HERNÁNDEZ *et al.* 2012). While this has not yet been described, in *C. elegans*, our results
690 support those findings. The FRAP experiments demonstrated that *de novo* GFP::SYS-1 plateaus around
691 6 to 8 minutes which suggests its stabilization is temporally limited in the E cell (Fig. 1D), and this could
692 be due to function of the destruction complex. Additionally, the partial depletion of APR-1 via RNAi in our
693 experiments seems to lower the steady state of degradation happening when Wnt-signaling is present,
694 which supports the observed role for the destruction complex in the E cell.
695 While our studies focused on the EMS daughter cells, previous studies showed that in both the
696 daughters of E (Ea and Ep) and MS (MSa and MSp), SYS-1 asymmetry is lost after *apr-1*(RNAi) (HUANG
697 *et al.* 2007). These results further support the idea that APR-1 regulation is key to maintain daughter cell
698 asymmetry and its role in both E, the Wnt-signaled daughter cell and MS, the unsignaled cell. In addition,
699 it has been previously shown that the observed asymmetry is not due to nuclear export or differential
700 subcellular distribution of SYS-1, but to the proteasomal degradation (HUANG *et al.* 2007). These data

701 suggests that SYS-1 asymmetry is tightly regulated by proteasomal degradation via mother cell
702 centrosomal processing and the destruction complex function in the EMS daughters.
703
704 Is SYS-1 inheritance the memory mechanism?
705 We observe that the rate of DENDRA2::SYS-1 clearance increases/scales with higher levels of
706 inherited DENDRA2::SYS-1 resulting in a tendency to return to basal levels over time (Table 1), which
707 suggests that SYS-1 inheritance itself is not causative in the enrichment of SYS-1 observed previously in
708 signaled cousins (ZACHARIAS *et al.* 2015). In addition to SYS-1 cousin enrichment, consistent lineage-
709 dependent changes in POP-1/TCF and WRM-1/β-catenin levels demonstrate that Wnt signaled
710 daughters of Wnt signaled cells respond more strongly to Wnt signaling in subsequent divisions
711 compared to their cousins that have fewer Wnt signaled cells in their lineage (ZACHARIAS *et al.* 2015;
712 ZACHARIAS AND MURRAY 2016). The observed enrichment in signaling status could be due to the
713 asymmetric localization or activation of upstream Wnt pathway components, including the Frizzled
714 receptor or the Dishevelled scaffold protein, which have been observed to be asymmetrically localized in
715 Wnt-dependent ACDs in the early embryo (PARK *et al.* 2004) and the seam lineage (MIZUMOTO AND
716 SAWA 2007; HUGHES *et al.* 2013; BALDWIN AND PHILLIPS 2014; SUGIOKA *et al.* 2018). A continued
717 asymmetric inheritance over multiple ACDs might then lead to skewed activation/accumulation of other
718 Wnt pathway components. In addition, this model cannot exclude the biased inheritance of post-
719 translational modification states, such as phosphorylation, and their effect on SYS-1 or other proteins
720 that regulate Wnt activity (ZACHARIAS *et al.* 2015)(Zacharias *et al*., 2015). Together, these data suggest
721 that though proper regulation of SYS-1 inheritance, as well as context-dependent regulation of inherited
722 SYS-1 in daughters, are key for a successful ACD and acquisition of different cell fates, SYS-1
723 inheritance itself is unlikely to be the basis for the “memory”, that allows cell that have been repeatedly
724 signaled to enrich SYS-1 in the nucleus.
725 Our proposed mechanism of SYS-1 regulation and inheritance during ACD sheds light into how
726 tightly regulated ACD processes are and the several layers of negative regulation needed for proper
727 SYS-1 nuclear levels in the daughter cells and further target gene activation. Indeed, trafficking and

degradation of mother cell SYS maintains asymmetric SYS-1 levels in the daughters at a level that can be effectively regulated by the destruction complex.

Acknowledgments

We thank Kimberly Bekas, Emily Hirsh and Amy Clemons for critical thinking and comments on the manuscript. Strains were provided by the Caenorhabditis Genetics Center, which is funded by the National Institutes of Health (NIH) Office of Research Infrastructure Programs (P40 OD01440). We also want to thank the Carver Center for Imaging in the Biology department of the University of Iowa and its director, Dr. Michael Dailey. This work was supported by NIH award RO1GM114007 (to B.T.P), and University of Iowa Graduate College Research Fellowships to M.V.

740 **References**


741 Bajaj, J., B. Zimdahl and T. Reya, 2015 Fearful symmetry: subversion of asymmetric division in cancer
742 development and progression. Cancer Res 75: 792-797.
743 Baldwin, A. T., A. M. Clemons and B. T. Phillips, 2016 Unique and redundant β-catenin regulatory roles of
744 two Dishevelled paralogs during C. elegans asymmetric cell division. J Cell Sci 129: 983-993.
745 Baldwin, A. T., and B. T. Phillips, 2014 The tumor suppressor APC differentially regulates multiple β-
746 catenins through the function of axin and CKIα during C. elegans asymmetric stem cell divisions. J
747 Cell Sci 127: 2771-2781.
748 Barth, A. I., H. Y. Caro-Gonzalez and W. J. Nelson, 2008 Role of adenomatous polyposis coli (APC) and
749 microtubules in directional cell migration and neuronal polarization. Semin Cell Dev Biol 19: 245-
750 251.
751 Bekas, K. N., and B. T. Phillips, 2020 Generating reliable hypomorphic phenocopies by RNAi using long
752 dsRNA as diluent. MicroPubl Biol 2020.
753 Bertrand, V., and O. Hobert, 2009 Linking asymmetric cell division to the terminal differentiation
754 program of postmitotic neurons in C. elegans. Dev Cell 16: 563-575.
755 Brenner, S., 1974 The genetics of Caenorhabditis elegans. Genetics 77: 71-94.
756 Chen, G., S. Yin, H. Zeng, H. Li and X. Wan, 2022 Regulation of Embryonic Stem Cell Self-Renewal. Life
757 (Basel) 12.
758 Chhabra, S. N., and B. W. Booth, 2021 Asymmetric cell division of mammary stem cells. Cell Div 16: 5.
759 Christian, J. L., 2012 Morphogen gradients in development: from form to function. Wiley Interdiscip Rev
760 Dev Biol 1: 3-15.
761 Chudakov, D. M., S. Lukyanov and K. A. Lukyanov, 2007 Using photoactivatable fluorescent protein
762 Dendra2 to track protein movement. Biotechniques 42: 553, 555, 557 passim.
763 Clevers, H., and R. Nusse, 2012 Wnt/β-catenin signaling and disease. Cell 149: 1192-1205.
764 Conte, D., Jr., L. T. MacNeil, A. J. M. Walhout and C. C. Mello, 2015 RNA Interference in Caenorhabditis
765 elegans. Curr Protoc Mol Biol 109: 26.23.21-26.23.30.
766 de la Roche, M., J. Worm and M. Bienz, 2008 The function of BCL9 in Wnt/beta-catenin signaling and
767 colorectal cancer cells. BMC Cancer 8: 199.
768 Giles, R. H., J. H. van Es and H. Clevers, 2003 Caught up in a Wnt storm: Wnt signaling in cancer. Biochim
769 Biophys Acta 1653: 1-24.
770 Goldstein, B., 1992 Induction of gut in Caenorhabditis elegans embryos. Nature 357: 255-257.
771 Habib, S. J., and S. P. Acebrón, 2022 Wnt signalling in cell division: from mechanisms to tissue
772 engineering. Trends Cell Biol 32: 1035-1048.
773 Harrell, J. R., and B. Goldstein, 2011 Internalization of multiple cells during C. elegans gastrulation
774 depends on common cytoskeletal mechanisms but different cell polarity and cell fate regulators.
775 Dev Biol 350: 1-12.
776 Hayat, R., M. Manzoor and A. Hussain, 2022 Wnt signaling pathway: A comprehensive review. Cell Biol
777 Int 46: 863-877.
778 Hernández, A. R., A. M. Klein and M. W. Kirschner, 2012 Kinetic responses of β-catenin specify the sites
779 of Wnt control. Science 338: 1337-1340.
780 Huang, S., P. Shetty, S. M. Robertson and R. Lin, 2007 Binary cell fate specification during C. elegans
781 embryogenesis driven by reiterated reciprocal asymmetry of TCF POP-1 and its coactivator beta-
782 catenin SYS-1. Development 134: 2685-2695.

783 Hughes, S., C. Brabin, P. J. Appleford and A. Woollard, 2013 CEH-20/Pbx and UNC-62/Meis function
784 upstream of rnt-1/Runx to regulate asymmetric divisions of the C. elegans stem-like seam cells.
785 Biol Open 2: 718-727.
786 Kamath, R. S., A. G. Fraser, Y. Dong, G. Poulin, R. Durbin *et al.*, 2003 Systematic functional analysis of the
787 Caenorhabditis elegans genome using RNAi. Nature 421: 231-237.
788 Kidd, A. R., 3rd, J. A. Miskowski, K. R. Siegfried, H. Sawa and J. Kimble, 2005 A beta-catenin identified by
789 functional rather than sequence criteria and its role in Wnt/MAPK signaling. Cell 121: 761-772.
790 Kochendoerfer, A. M., F. Modafferi and E. M. Dunleavy, 2021 Centromere function in asymmetric cell
791 division in Drosophila female and male germline stem cells. Open Biol 11: 210107.
792 Lam, A. K., and B. T. Phillips, 2017 Wnt Signaling Polarizes C. elegans Asymmetric Cell Divisions During
793 Development. Results Probl Cell Differ 61: 83-114.
794 Leggett, D. S., J. Hanna, A. Borodovsky, B. Crosas, M. Schmidt *et al.*, 2002 Multiple associated proteins
795 regulate proteasome structure and function. Mol Cell 10: 495-507.
796 Lehmann, A., A. Niewienda, K. Jechow, K. Janek and C. Enenkel, 2010 Ecm29 fulfils quality control
797 functions in proteasome assembly. Mol Cell 38: 879-888.
798 Lin, R., R. J. Hill and J. R. Priess, 1998 POP-1 and anterior-posterior fate decisions in C. elegans embryos.
799 Cell 92: 229-239.
800 Lo, M. C., F. Gay, R. Odom, Y. Shi and R. Lin, 2004 Phosphorylation by the beta-catenin/MAPK complex
801 promotes 14-3-3-mediated nuclear export of TCF/POP-1 in signal-responsive cells in C. elegans.
802 Cell 117: 95-106.
803 MacDonald, B. T., K. Tamai and X. He, 2009 Wnt/beta-catenin signaling: components, mechanisms, and
804 diseases. Dev Cell 17: 9-26.
805 Mizumoto, K., and H. Sawa, 2007 Cortical beta-catenin and APC regulate asymmetric nuclear beta-
806 catenin localization during asymmetric cell division in C. elegans. Dev Cell 12: 287-299.
807 Morrison, S. J., and J. Kimble, 2006 Asymmetric and symmetric stem-cell divisions in development and
808 cancer. Nature 441: 1068-1074.
809 Murgan, S., W. Kari, U. Rothbächer, M. Iché-Torres, P. Mélénec *et al.*, 2015 Atypical Transcriptional
810 Activation by TCF via a Zic Transcription Factor in C. elegans Neuronal Precursors. Dev Cell 33:
811 737-745.
812 Neumüller, R. A., and J. A. Knoblich, 2009 Dividing cellular asymmetry: asymmetric cell division and its
813 implications for stem cells and cancer. Genes Dev 23: 2675-2699.
814 Obrador-Hevia, A., S. F. Chin, S. González, J. Rees, F. Vilardell *et al.*, 2010 Oncogenic KRAS is not
815 necessary for Wnt signalling activation in APC-associated FAP adenomas. J Pathol 221: 57-67.
816 Park, F. D., J. R. Tenlen and J. R. Priess, 2004 C. elegans MOM-5/frizzled functions in MOM-2/Wnt-
817 independent cell polarity and is localized asymmetrically prior to cell division. Curr Biol 14: 2252-
818 2258.
819 Peel, N., M. Dougherty, J. Goeres, Y. Liu and K. F. O'Connell, 2012 The C. elegans F-box proteins LIN-23
820 and SEL-10 antagonize centrosome duplication by regulating ZYG-1 levels. J Cell Sci 125: 3535-
821 3544.
822 Phillips, B. T., A. R. Kidd, 3rd, R. King, J. Hardin and J. Kimble, 2007 Reciprocal asymmetry of SYS-1/beta-
823 catenin and POP-1/TCF controls asymmetric divisions in Caenorhabditis elegans. Proc Natl Acad
824 Sci U S A 104: 3231-3236.
825 Phillips, B. T., and J. Kimble, 2009 A new look at TCF and beta-catenin through the lens of a divergent C.
826 elegans Wnt pathway. Dev Cell 17: 27-34.
827 Polakis, P., 2012 Wnt signaling in cancer. Cold Spring Harb Perspect Biol 4.

Qu, Y., N. Gharbi, X. Yuan, J. R. Olsen, P. Blicher *et al.*, 2016 Axitinib blocks Wnt/β-catenin signaling and directs asymmetric cell division in cancer. Proc Natl Acad Sci U S A 113**:** 9339-9344.

Quyn, A. J., P. L. Appleton, F. A. Carey, R. J. Steele, N. Barker *et al.*, 2010 Spindle orientation bias in gut epithelial stem cell compartments is lost in precancerous tissue. Cell Stem Cell 6**:** 175-181.

Ring, A., Y. M. Kim and M. Kahn, 2014 Wnt/catenin signaling in adult stem cell physiology and disease. Stem Cell Rev Rep 10**:** 512-525.

Robertson, S. M., and R. Lin, 2012 Our evolving view of Wnt signaling in C. elegans: If two's company and three's a crowd, is four really necessary? Worm 1**:** 82-89.

Rocheleau, C. E., W. D. Downs, R. Lin, C. Wittmann, Y. Bei *et al.*, 1997 Wnt signaling and an APC-related gene specify endoderm in early C. elegans embryos. Cell 90**:** 707-716.

Rocheleau, C. E., J. Yasuda, T. H. Shin, R. Lin, H. Sawa *et al.*, 1999 WRM-1 activates the LIT-1 protein kinase to transduce anterior/posterior polarity signals in C. elegans. Cell 97**:** 717-726.

Sawa, H., and H. C. Korswagen, 2013 Wnt signaling in C. elegans. WormBook**:** 1-30.

Sawa, H., L. Lobel and H. R. Horvitz, 1996 The Caenorhabditis elegans gene lin-17, which is required for certain asymmetric cell divisions, encodes a putative seven-transmembrane protein similar to the Drosophila frizzled protein. Genes Dev 10**:** 2189-2197.

Schlaitz, A. L., M. Srayko, A. Dammermann, S. Quintin, N. Wielsch *et al.*, 2007 The C. elegans RSA complex localizes protein phosphatase 2A to centrosomes and regulates mitotic spindle assembly. Cell 128**:** 115-127.

Sugioka, K., L. E. Fielmich, K. Mizumoto, B. Bowerman, S. van den Heuvel *et al.*, 2018 Tumor suppressor APC is an attenuator of spindle-pulling forces during C. elegans asymmetric cell division. Proc Natl Acad Sci U S A 115**:** E954-e963.

Sugioka, K., K. Mizumoto and H. Sawa, 2011 Wnt regulates spindle asymmetry to generate asymmetric nuclear β-catenin in C. elegans. Cell 146**:** 942-954.

Thompson, J. W., M. F. V. Michel and B. T. Phillips, 2022 Centrosomal enrichment and proteasomal degradation of SYS-1/β-catenin requires the microtubule motor dynein. Mol Biol Cell 33**:** ar42.

Timmons, L., 2006 Delivery methods for RNA interference in C. elegans. Methods Mol Biol 351**:** 119-125.

Umbhauer, M., A. Djiane, C. Goisset, A. Penzo-Méndez, J. F. Riou *et al.*, 2000 The C-terminal cytoplasmic Lys-thr-X-X-X-Trp motif in frizzled receptors mediates Wnt/beta-catenin signalling. Embo j 19**:** 4944-4954.

Vora, S., and B. T. Phillips, 2015 Centrosome-Associated Degradation Limits β-Catenin Inheritance by Daughter Cells after Asymmetric Division. Curr Biol 25**:** 1005-1016.

Vora, S. M., and B. T. Phillips, 2016 The benefits of local depletion: The centrosome as a scaffold for ubiquitin-proteasome-mediated degradation. Cell Cycle 15**:** 2124-2134.

Woods, E., J. Courtney, D. Scholz, W. W. Hall and V. W. Gautier, 2014 Tracking protein dynamics with photoconvertible Dendra2 on spinning disk confocal systems. J Microsc 256**:** 197-207.

Yamashita, Y. M., H. Yuan, J. Cheng and A. J. Hunt, 2010 Polarity in stem cell division: asymmetric stem cell division in tissue homeostasis. Cold Spring Harb Perspect Biol 2**:** a001313.

Yang, X. D., T. R. Karhadkar, J. Medina, S. M. Robertson and R. Lin, 2015 β-Catenin-related protein WRM-1 is a multifunctional regulatory subunit of the LIT-1 MAPK complex. Proc Natl Acad Sci U S A 112**:** E137-146.

Zacharias, A. L., and J. I. Murray, 2016 Combinatorial decoding of the invariant C. elegans embryonic lineage in space and time. Genesis 54**:** 182-197.

Zacharias, A. L., T. Walton, E. Preston and J. I. Murray, 2015 Quantitative Differences in Nuclear β-catenin and TCF Pattern Embryonic Cells in C. elegans. PLoS Genet 11**:** e1005585.

874
875
876

877 **Figure legends**
878
879 **Figure 1: Photobleaching reveals *de novo* and inherited SYS-1 pools in the E and MS cells and**
880 **centrosomal SYS-1 dynamics over time.** A) Diagram of EMS cell Fluorescence After Photobleaching
881 (FRAP) assay. The EMS cell is polarized by Wnt signaling from the P2 cell. The entire EMS mother cell
882 is photobleached and SYS-1 nuclear levels are subsequently measured throughout the development of
883 the E and the MS daughters. B) Quantification of nuclear SYS-1::GFP in E and MS cells following no
884 photobleach (n=8), and photobleaching at anaphase (n=12), telophase (n=11), and cytokinesis (n=10).
885 Fluorescence recordings were measured 4 min after mother cell division is complete. Mean +/- SEM.
886 Student's two-tail t-test. C) Photobleaching protocol for panel D) and C). D)Quantification of nuclear
887 fluorescent SYS-1::GFP in the E and MS cells over time in non-bleached controls and EMS cell
888 photobleached at cytokinesis. Mean +/- SEM. Student's two-tail t-test. E) Percentage of nuclear SYS-1 in
889 the daughter cells during a 2 min interval timecourse elucidates *de novo* translated SYS-1 dynamics in
890 the E and MS daughter cells over time. N= denoted by grey figures in graph. * $p \leq 0.05$, ** $p \leq 0.01$, *** $p$
891 $\leq 0.001$, **** $p \leq 0.0001$
892
893
894

**Figure 2: <u>Photoconversion of DENDRA2::SYS-1 reveals turnover at the centrosome during mitosis.</u>**
A) Pre-conversion image shows centrosomal localization of DENDRA2::SYS-1 in the green channel. B) Centrosomal DENDRA2::SYS-1 is undetectable in the red channel prior to photoconversion by 405nm blue laser exposure. C) After photoconversion newly translated DENDRA2::SYS-1 is trafficked to the centrosome, and D) shows photoconverted DENDRA2::SYS-1 at the centrosome. E) Photoconversion protocol for centrosomal DENDRA2::SYS-1 timecourse. F) Quantification of average centrosomal DENDRA2::SYS-1 in both channels over time. Mean +/- SEM. N=3. G) Centrosomal enrichment index (CEI) of the time course shown in (F). Mean +/- SEM. N=3. CEI was calculated in FIJI by subtracting the mean pixel intensity of a cytoplasmic ROI encompassing the posterior half of the cell with the dotted white line (A–D), from a circular centrosome ROI.

908 **Figure 3: <u>Photoconversion of the cytoplasm of the P1 cell unveils dynamics of dynein trafficking</u>**
909 **<u>of DENDRA2::SYS-1 during mitosis.</u>**

910 A) Diagram of photoconversion of the P1 cell. Dotted square represents the photoconverted area of the
911 cytoplasm at metaphase. B) Photoconversion protocol for cytoplasm photoconversion in C), D), and E).
912 C) Quantification of raw DENDRA2::SYS-1 of the distal and proximal centrosome in green and red
913 channels pre- and post-photoconversion of the cytoplasm, measured over a 2 min. timecourse in 20 s
914 intervals after photoconversion on control *lacZ*(RNAi). Mean +/-SEM. N=12. D) Quantification of
915 DENDRA2::SYS-1 of the distal and proximal centrosome in red channel pre- and post-photoconversion
916 of the cytoplasm, measured over a 2 min. timecourse in 20 s intervals after photoconversion on control
917 *lacZ*(RNAi). Mean +/-SEM. N=12. E) Timecourse depicting red, photoconverted DENDRA2::SYS-1 CEI
918 on *lacZ*(RNAi) and *dlc-1*(RNAi). Mean +/-SEM. N= 12 and 15, respectively.

919

920 **Figure 4: <u>E and MS inheritance of mother cell SYS-1 is limited by EMS centrosomal processing.</u>**
921 A) Photoconversion protocol for quantification of nuclear inherited DENDRA2::SYS-1 timecourse. B)
922 Quantification of inherited, red DENDRA2::SYS-1 nuclear levels of the E and MS cells at different
923 timepoints starting 2 m after cytokinesis of the EMS mother cell in 60 second increments on the control
924 *lacZ*(RNAi). Mean +/-SEM. 2way ANOVA followed by Tukey Mixed effects analysis in Multiple
925 Comparisons test. N=12. C) Quantification of inherited, red DENDRA2::SYS-1 nuclear levels of the E
926 and MS cells timecourse on control vs. *dlc-1*(RNAi) (N=26 and N=20, respectively). Mean +/-SEM. 2way
927 ANOVA followed by Sidak Mixed effects analysis in Multiple Comparisons test. D) Quantification of
928 inherited, red DENDRA2::SYS-1 nuclear levels of the E and MS daughter cells timecourse on control vs.
929 *rsa-2*(RNAi) (N=26 and N=20, respectively). Mean +/-SEM. 2way ANOVA followed by Sidak Mixed
930 effects analysis in Multiple Comparisons test. E) Quantification of inherited, red DENDRA2::SYS-1
931 nuclear levels of the E and MS daughter cells timecourse on control vs. *ecps-1*(RNAi) (n=26 and n=20,
932 respectively). Mean +/-SEM. 2way ANOVA followed by Sidak Mixed effects analysis in Multiple
933 Comparisons test. F) Quantification of fold change in asymmetry between the E and MS cells in *lacZ,*
934 *dlc-1, rsa-2 and ecps-1,* (RNAi). DENDRA2::SYS-1 fluorescent intensity was calculated by subtracting
935 N2 fluorescence at all different timepoints. * represent the P-value when comparing the averaged value
936 of all time points of *lacZ(*RNAi) to experimental condition. Table S1. P-values when comparing each time
937 point. * $p \leq 0.05$, ** $p \leq 0.01$, *** $p \leq 0.001$, **** $p \leq 0.0001$

938
939
940

**Figure 5: <u>Loss of centrosomal SYS-1 results in increased levels of nuclear *de novo* SYS-1 in EMS daughter cells</u>.** A) Photoconversion protocol for quantification of nuclear inherited DENDRA2::SYS-1 timecourse. B) Quantification of green/*de novo* SYS-1 nuclear levels in the E and MS cells after photoconversion of the EMS cell at cytokinesis; the timecourse depicts SYS-1 nuclear levels at different timepoints starting 2 minutes after cytokinesis of the EMS cell in 60 second increments on the control *lacZ*(RNAi) (n=26). Mean+/- SEM. 2way ANOVA followed by Sidak Mixed effects analysis in Multiple Comparisons test. C) Quantification of *de novo* SYS-1 nuclear levels of the E and MS cells timecourse on *lacZ(RNAi)* and *dlc-1*(RNAi) (n=26 and n=20, respectively). Mean +/-SEM. 2way ANOVA followed by Sidak Mixed effects analysis in Multiple Comparisons test. D) Quantification of *de novo* SYS-1 nuclear levels of the E and MS cells timecourse on *lacZ(RNAi)* and *rsa-2*(RNAi) (n=26 and n=20, respectively). Mean +/-SEM. 2way ANOVA followed by Sidak Mixed effects analysis in Multiple Comparisons test. E) Quantification of *de novo* SYS-1 nuclear levels of the E and MS cells timecourse on *lacZ(RNAi)* and *ecps-1*(RNAi) (n=26 and n=20, respectively). Mean+/- SEM. 2way ANOVA followed by Sidak Mixed effects analysis in Multiple Comparisons test. F) Quantification of fold change in asymmetry between the E and MS daughter cell in *lacZ, dlc-1, rsa-2 and ecps-1* (RNAi). DENDRA2::SYS-1 fluorescent intensity was calculated by subtracting N2 fluorescence at all different timepoints. * represent the P-value when comparing all time points and the average of control to experimental condition. Table S1. P-values when comparing each time point. * $p \leq 0.05$, ** $p \leq 0.01$, *** $p \leq 0.001$, **** $p \leq 0.0001$

963 **Figure 6: <u>Partial loss of the negative regulator of the Wnt signaling pathway, APR-1, affects both</u>**
964 **<u>pools of nuclear SYS-1 in the E and MS cells</u>.** A) Quantification of *de novo* SYS-1 nuclear levels in the
965 E and MS cells after photoconversion at cytokinesis over 7-minute timecourse on *lacZ(RNAi) and apr-1*
966 (RNAi) (n=26 and n=20, respectively). Mean +/-SEM. 2way ANOVA followed by Sidak Mixed effects
967 analysis in Multiple Comparisons test. B) Quantification of inherited SYS-1 nuclear levels in the E and
968 MS cells after photoconversion at cytokinesis over 7-minute timecourse on *lacZ(RNAi) and apr-1* (RNAi).
969 Mean +/-SEM. 2way ANOVA followed by Sidak Mixed effects analysis in Multiple Comparisons test. C)
970 Graph representation of the fold change in *de* novo and inherited nuclear SYS-1 of APR-1 compared to
971 the control in the E and MS cells. D) Quantification of centrosomal DENDRA2::SYS-1 levels during
972 telophase in the EMS cell on *lacZ(RNAi)* and *apr-1* (RNAi) (n=20 and n=18, respectively). Mean +/-SEM.
973 Unpaired two-tail t-test. * represent the P-value when comparing all time points and the average of
974 control to experimental condition. Table S1. P-values when comparing each time point. DENDRA2::SYS-
975 1 fluorescent intensity was calculated by subtracting N2 fluorescence at all different timepoints. * $p \leq$
976 $0.05$, ** $p \leq 0.01$, *** $p \leq 0.001$, **** $p \leq 0.0001$
977
978
979

**Figure 7: <u>Model for SYS-1 regulation during ACD</u>.** A) In wildtype, in the EMS cell, cytosolic SYS (green) is trafficked to the centrosome via dynein where it gets degraded by the centrosomal proteosome. The remaining cytosolic SYS-1 is inherited into the E and MS cells where it is regulated by APR-1. The inherited and the *de novo* pools in both daughter cells are freely exchanged, stably maintaining the pools through the cell cycle. In the MS cell, APR-1 lowers SYS-1 levels such that it is asymmetric compared to the E cell, which has reduced APR-1 activity. B) Loss of SYS-1 mother cell regulation, including loss of SYS-1 centrosomal trafficking, coupling or degradation, decreases degradation of the cytosolic SYS-1 at the centrosome, leading to increased SYS-1 inheritance into both daughter cells (bold arrows). In the E and MS cell the increased inherited SYS-1 leads to an increased *de novo* pool. APR-1 is unable to bring SYS-1 levels down to basal levels, which leads to higher levels of both SYS-1 pools and a loss of SYS-1 asymmetry between the E and MS cell. C) Loss of APR-1 has no effect in the EMS cell, however, APR-1 depletion leads to an increased *de novo* SYS-1 pool, which in turn, affects the inherited pool, since the cell is unable to bring SYS-1 back to basal levels in both daughters. Higher levels of both pools in the E and MS nuclei lead to a loss of SYS-1 asymmetry. The weight of the arrows and lines represent the relative changed effect, font size represents size of the relevant SYS-1 pool. SYS-$1^{i}$, inherited SYS-1; SYS-$1^{dn}$, *de novo* SYS-1. D) During cytokinesis of the EMS cell, the Wnt gradient polarizes the cell leading to differential accumulation of SYS-1 and APR-1 on opposite sides of the cell. The posterior part of the cell becomes the signaled E cell and has more inherited SYS-1 and less APR-1 . The anterior side will have more APR-1 and less inherited SYS-1. E) From the formation of the nucleus (2min) up to 6min. after cytokinesis, the MS cell will have active negative regulation of total SYS-1 (inherited and *de novo* SYS-1) via APR-1. In the E cell, total SYS-1 increases due to lack of negative regulation via APR-1. F) From 8 to 10 minutes after cytokinesis the APR-1 present in the E cell is active and negatively regulates total SYS-1. In the MS cell, negative regulation of SYS-1 via APR-1 continues.

Figure 1

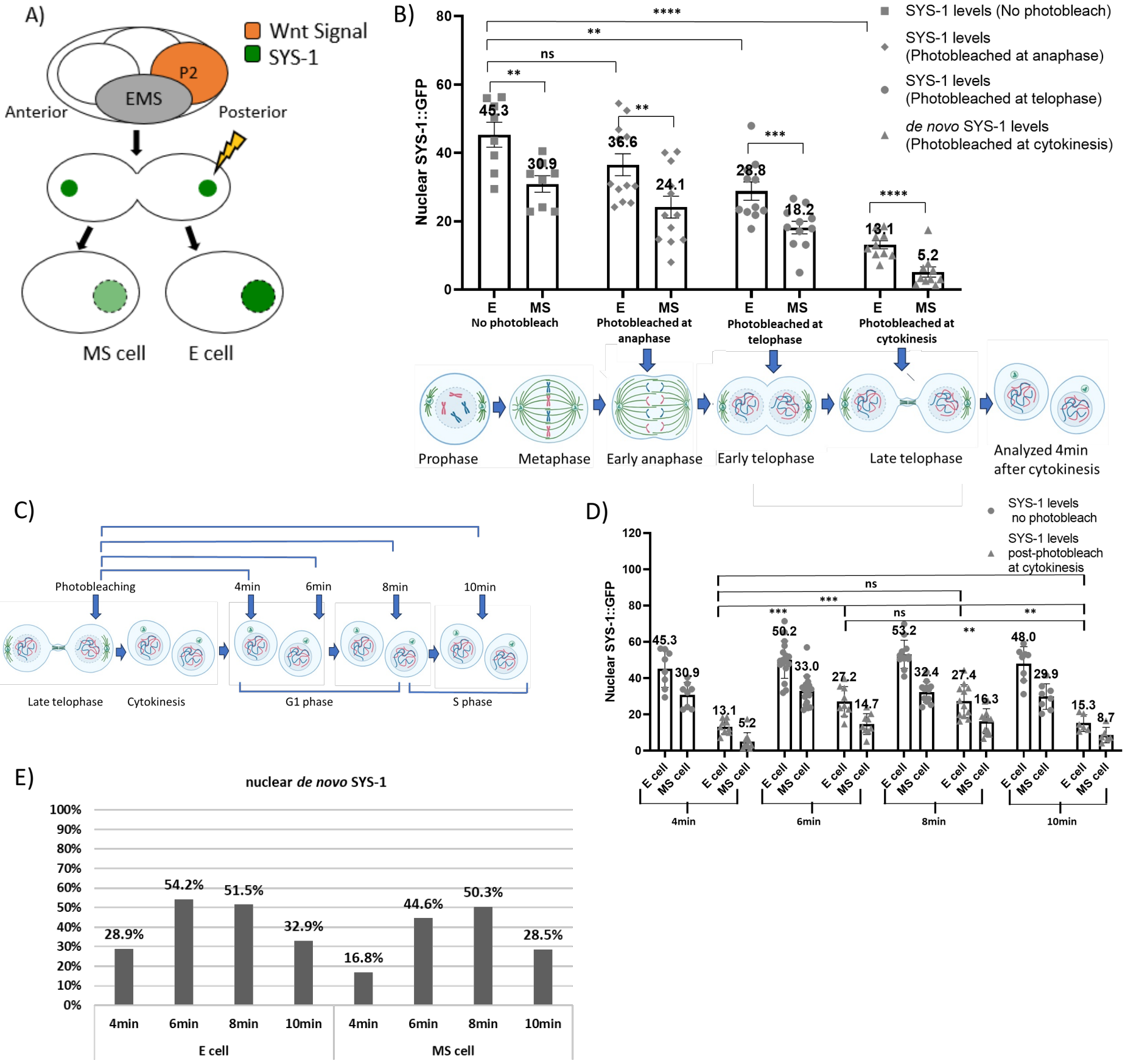
A)
Wnt Signal
SYS-1
P2
EMS
Anterior
Posterior
MS cell
E cell
B)
Nuclear SYS-1::GFP
SYS-1 levels (No photobleach)
SYS-1 levels (Photobleached at anaphase)
SYS-1 levels (Photobleached at telophase)
de novo SYS-1 levels (Photobleached at cytokinesis)
45.3
30.9
36.6
24.1
28.8
18.2
13.1
5.2
E MS
No photobleach
Photobleached at anaphase
Photobleached at telophase
Photobleached at cytokinesis
Prophase
Metaphase
Early anaphase
Early telophase
Late telophase
Analyzed 4min after cytokinesis
C)
Photobleaching
4min
6min
8min
10min
Late telophase
Cytokinesis
G1 phase
S phase
D)
Nuclear SYS-1::GFP
SYS-1 levels no photobleach
SYS-1 levels post-photobleach at cytokinesis
45.3
30.9
13.1
5.2
50.2
33.0
27.2
14.7
53.2
32.4
27.4
16.3
48.0
29.9
15.3
8.7
E cell
MS cell
4min
6min
8min
10min
E)
nuclear de novo SYS-1
28.9%
54.2%
51.5%
32.9%
16.8%
44.6%
50.3%
28.5%
4min
6min
8min
10min
E cell
MS cell

Figure 2

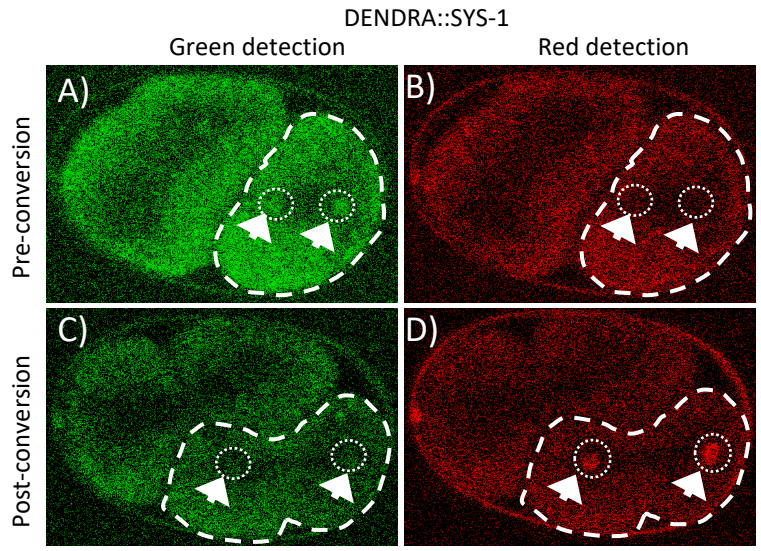
DENDRA::SYS-1
Green detection
Red detection
A)
B)
C)
D)
Pre-conversion
Post-conversion

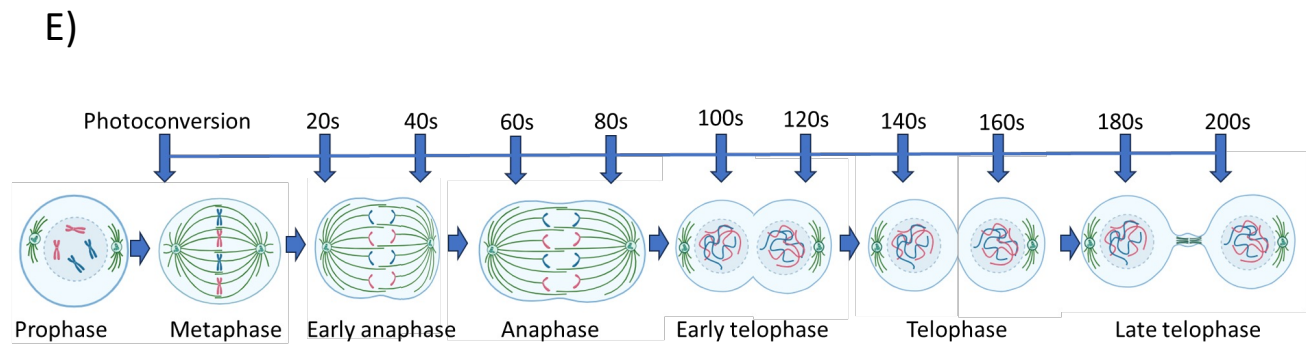
E)
Photoconversion
20s
40s
60s
80s
100s
120s
140s
160s
180s
200s
Prophase
Metaphase
Early anaphase
Anaphase
Early telophase
Telophase
Late telophase

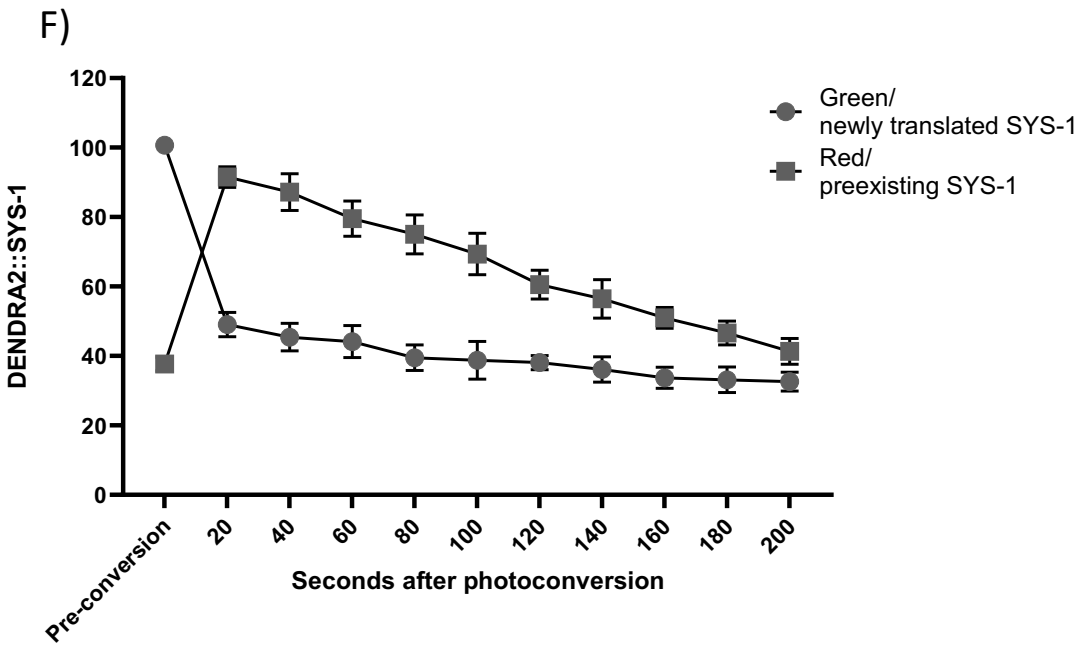
F)
DENDRA2::SYS-1
120
100
80
60
40
20
0
Pre-conversion
20
40
60
80
100
120
140
160
180
200
Seconds after photoconversion
Green/
newly translated SYS-1
Red/
preexisting SYS-1

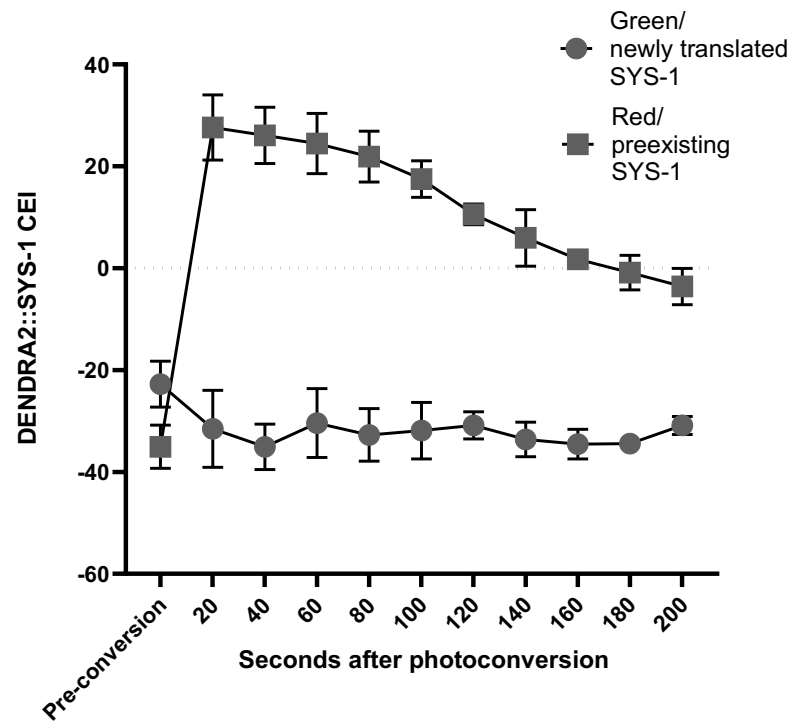
G)
DENDRA2::SYS-1 CEI
40
20
0
-20
-40
-60
Pre-conversion
20
40
60
80
100
120
140
160
180
200
Seconds after photoconversion
Green/
newly translated
SYS-1
Red/
preexisting
SYS-1

Figure 3

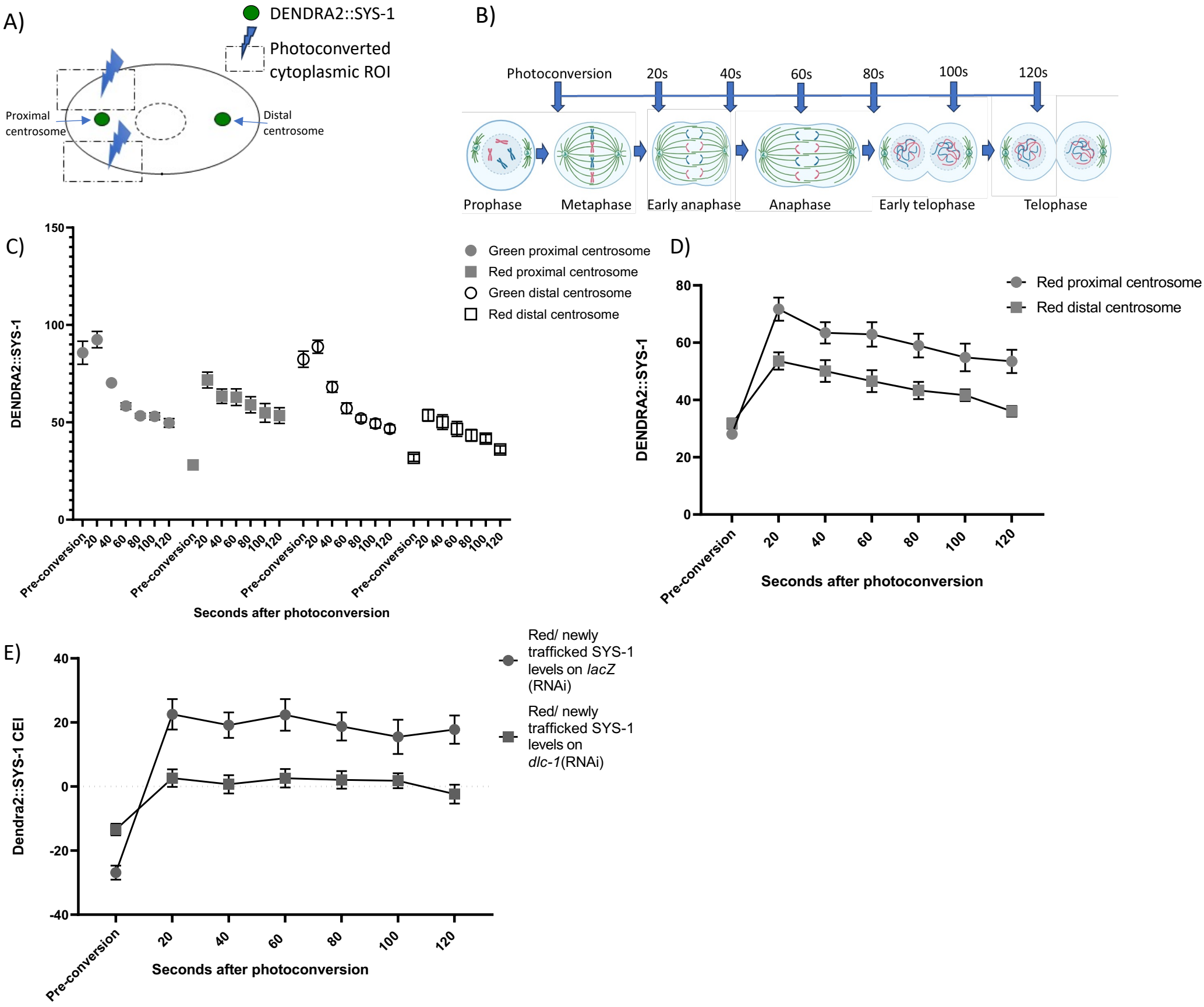
A)
DENDRA2::SYS-1
Photoconverted cytoplasmic ROI
Proximal centrosome
Distal centrosome
B)
Photoconversion
20s
40s
60s
80s
100s
120s
Prophase
Metaphase
Early anaphase
Anaphase
Early telophase
Telophase
C)
Green proximal centrosome
Red proximal centrosome
Green distal centrosome
Red distal centrosome
DENDRA2::SYS-1
Seconds after photoconversion
D)
Red proximal centrosome
Red distal centrosome
DENDRA2::SYS-1
Seconds after photoconversion
E)
Red/ newly trafficked SYS-1 levels on lacZ (RNAi)
Red/ newly trafficked SYS-1 levels on dlc-1(RNAi)
Dendra2::SYS-1 CEI
Seconds after photoconversion

Figure 4

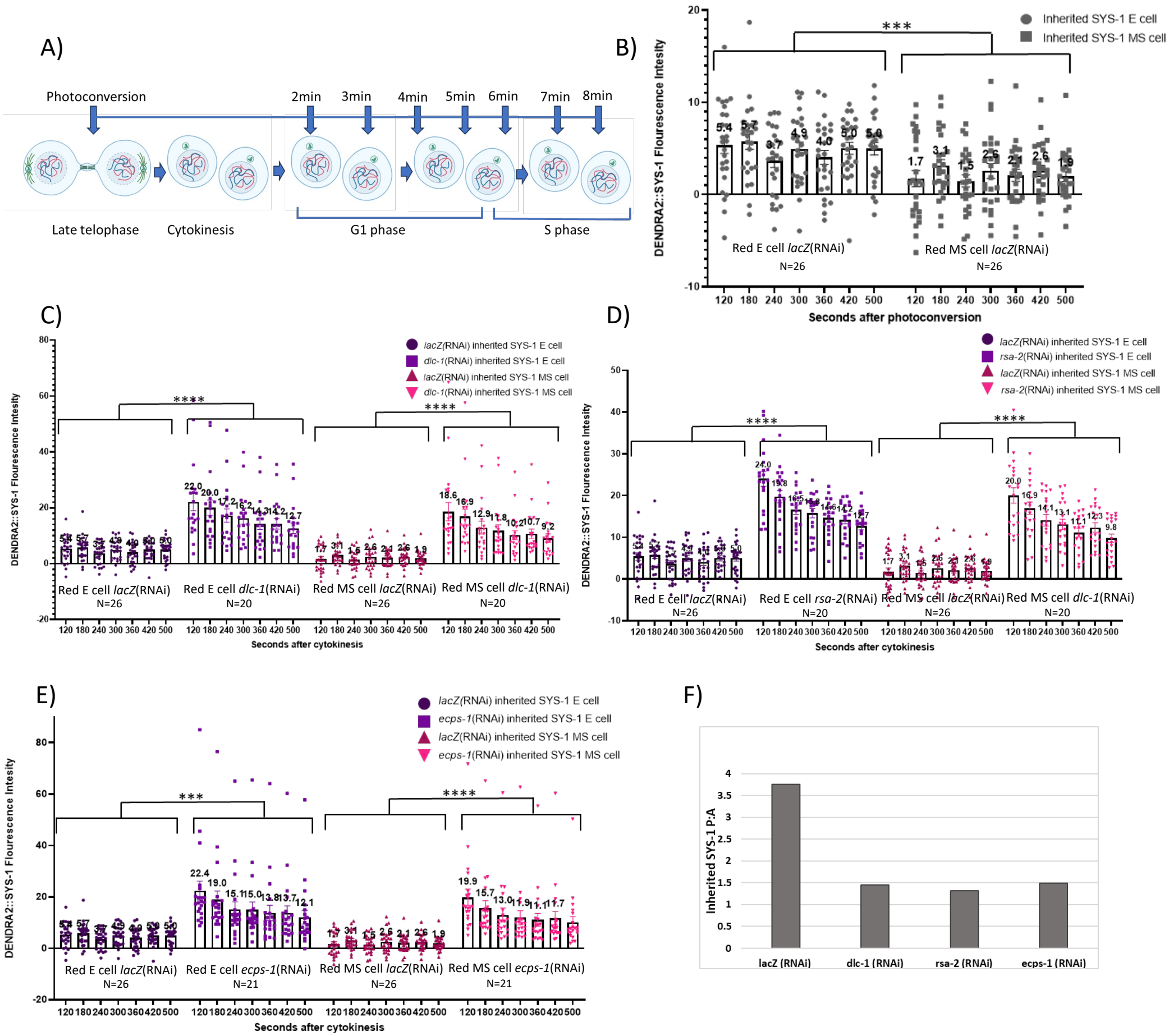
A)
Photoconversion
2min
3min
4min
5min
6min
7min
8min
Late telophase
Cytokinesis
G1 phase
S phase
B)
Inherited SYS-1 E cell
Inherited SYS-1 MS cell
DENDRA2::SYS-1 Flourescence Intesity
Red E cell lacZ(RNAi)
N=26
Red MS cell lacZ(RNAi)
N=26
Seconds after photoconversion
C)
lacZ(RNAi) inherited SYS-1 E cell
dlc-1(RNAi) inherited SYS-1 E cell
lacZ(RNAi) inherited SYS-1 MS cell
dlc-1(RNAi) inherited SYS-1 MS cell
Red E cell lacZ(RNAi)
N=26
Red E cell dlc-1(RNAi)
N=20
Red MS cell lacZ(RNAi)
N=26
Red MS cell dlc-1(RNAi)
N=20
Seconds after cytokinesis
D)
lacZ(RNAi) inherited SYS-1 E cell
rsa-2(RNAi) inherited SYS-1 E cell
lacZ(RNAi) inherited SYS-1 MS cell
rsa-2(RNAi) inherited SYS-1 MS cell
Red E cell lacZ(RNAi)
N=26
Red E cell rsa-2(RNAi)
N=20
Red MS cell lacZ(RNAi)
N=26
Red MS cell dlc-1(RNAi)
N=20
Seconds after cytokinesis
E)
lacZ(RNAi) inherited SYS-1 E cell
ecps-1(RNAi) inherited SYS-1 E cell
lacZ(RNAi) inherited SYS-1 MS cell
ecps-1(RNAi) inherited SYS-1 MS cell
Red E cell lacZ(RNAi)
N=26
Red E cell ecps-1(RNAi)
N=21
Red MS cell lacZ(RNAi)
N=26
Red MS cell ecps-1(RNAi)
N=21
Seconds after cytokinesis
F)
Inherited SYS-1 P:A
lacZ (RNAi)
dlc-1 (RNAi)
rsa-2 (RNAi)
ecps-1 (RNAi)

Figure 5

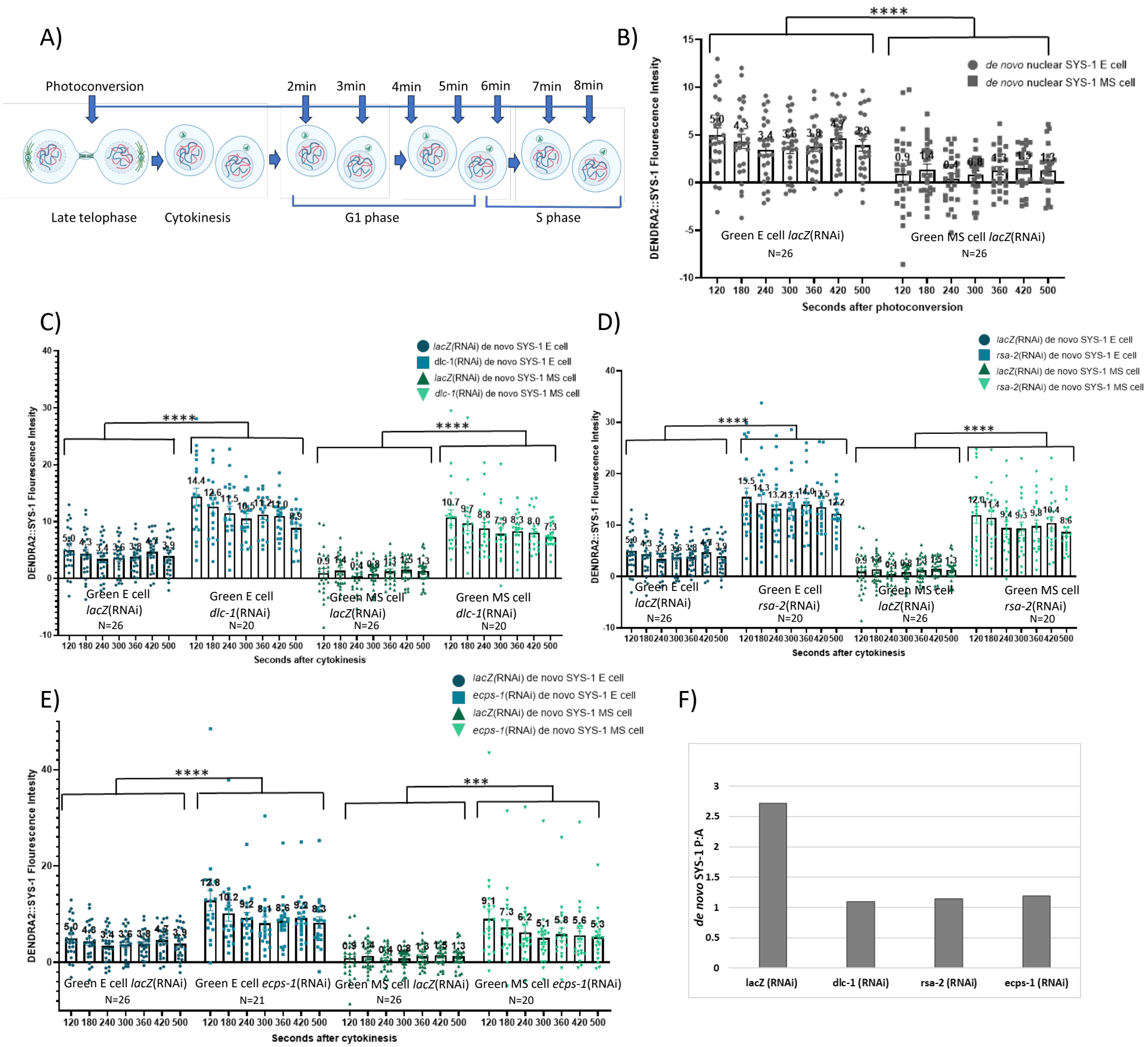
A)
Photoconversion
2min
3min
4min
5min
6min
7min
8min
Late telophase
Cytokinesis
G1 phase
S phase
B)
****
de novo nuclear SYS-1 E cell
de novo nuclear SYS-1 MS cell
DENDRA2::SYS-1 Flourescence Intesity
Green E cell lacZ(RNAi)
N=26
Green MS cell lacZ(RNAi)
N=26
Seconds after photoconversion
C)
lacZ(RNAi) de novo SYS-1 E cell
dlc-1(RNAi) de novo SYS-1 E cell
lacZ(RNAi) de novo SYS-1 MS cell
dlc-1(RNAi) de novo SYS-1 MS cell
Green E cell lacZ(RNAi) N=26
Green E cell dlc-1(RNAi) N=20
Green MS cell lacZ(RNAi) N=26
Green MS cell dlc-1(RNAi) N=20
Seconds after cytokinesis
D)
lacZ(RNAi) de novo SYS-1 E cell
rsa-2(RNAi) de novo SYS-1 E cell
lacZ(RNAi) de novo SYS-1 MS cell
rsa-2(RNAi) de novo SYS-1 MS cell
Green E cell lacZ(RNAi) N=26
Green E cell rsa-2(RNAi) N=20
Green MS cell lacZ(RNAi) N=26
Green MS cell rsa-2(RNAi) N=20
Seconds after cytokinesis
E)
lacZ(RNAi) de novo SYS-1 E cell
ecps-1(RNAi) de novo SYS-1 E cell
lacZ(RNAi) de novo SYS-1 MS cell
ecps-1(RNAi) de novo SYS-1 MS cell
***
Green E cell lacZ(RNAi) N=26
Green E cell ecps-1(RNAi) N=21
Green MS cell lacZ(RNAi) N=26
Green MS cell ecps-1(RNAi) N=20
Seconds after cytokinesis
F)
de novo SYS-1 P:A
lacZ (RNAi)
dlc-1 (RNAi)
rsa-2 (RNAi)
ecps-1 (RNAi)

Figure 6

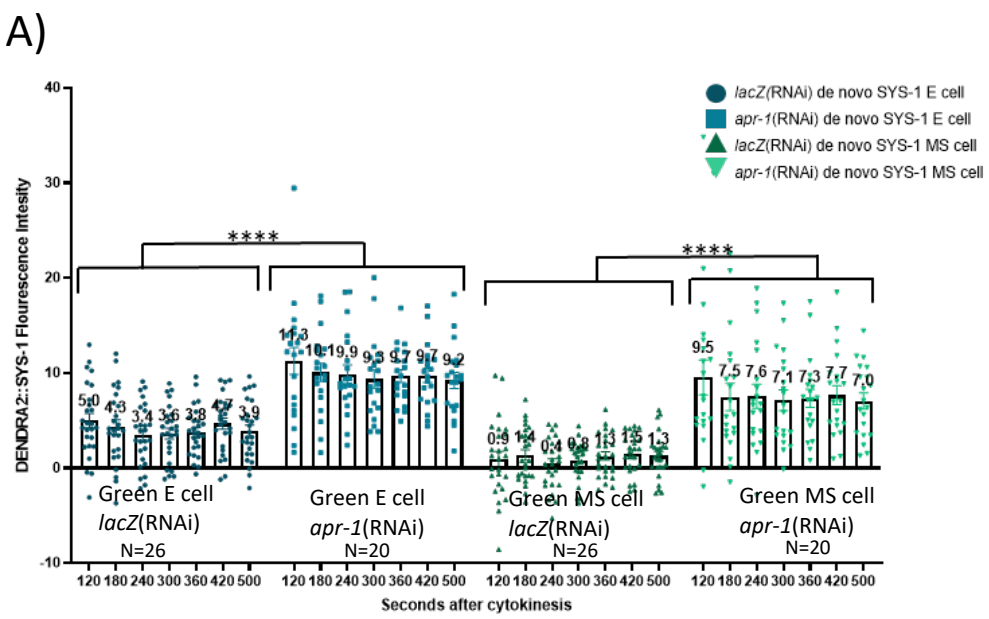
A)
lacZ(RNAi) de novo SYS-1 E cell
apr-1(RNAi) de novo SYS-1 E cell
lacZ(RNAi) de novo SYS-1 MS cell
apr-1(RNAi) de novo SYS-1 MS cell
DENDRA2::SYS-1 Flourescence Intesity
****
****
Green E cell lacZ(RNAi) N=26
Green E cell apr-1(RNAi) N=20
Green MS cell lacZ(RNAi) N=26
Green MS cell apr-1(RNAi) N=20
Seconds after cytokinesis

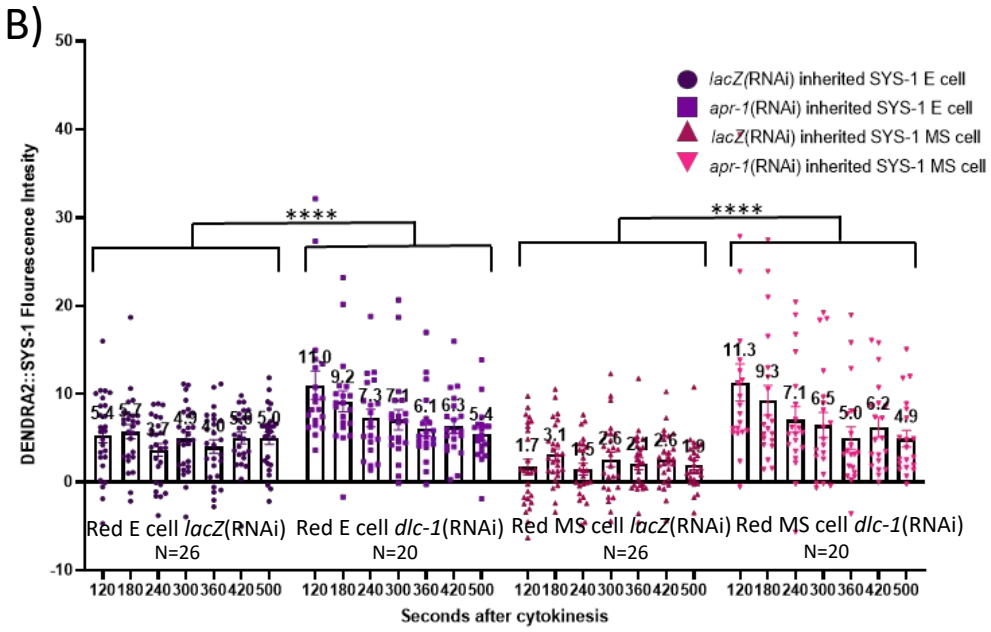
B)
lacZ(RNAi) inherited SYS-1 E cell
apr-1(RNAi) inherited SYS-1 E cell
lacZ(RNAi) inherited SYS-1 MS cell
apr-1(RNAi) inherited SYS-1 MS cell
DENDRA2::SYS-1 Flourescence Intesity
****
****
Red E cell lacZ(RNAi) N=26
Red E cell dlc-1(RNAi) N=20
Red MS cell lacZ(RNAi) N=26
Red MS cell dlc-1(RNAi) N=20
Seconds after cytokinesis

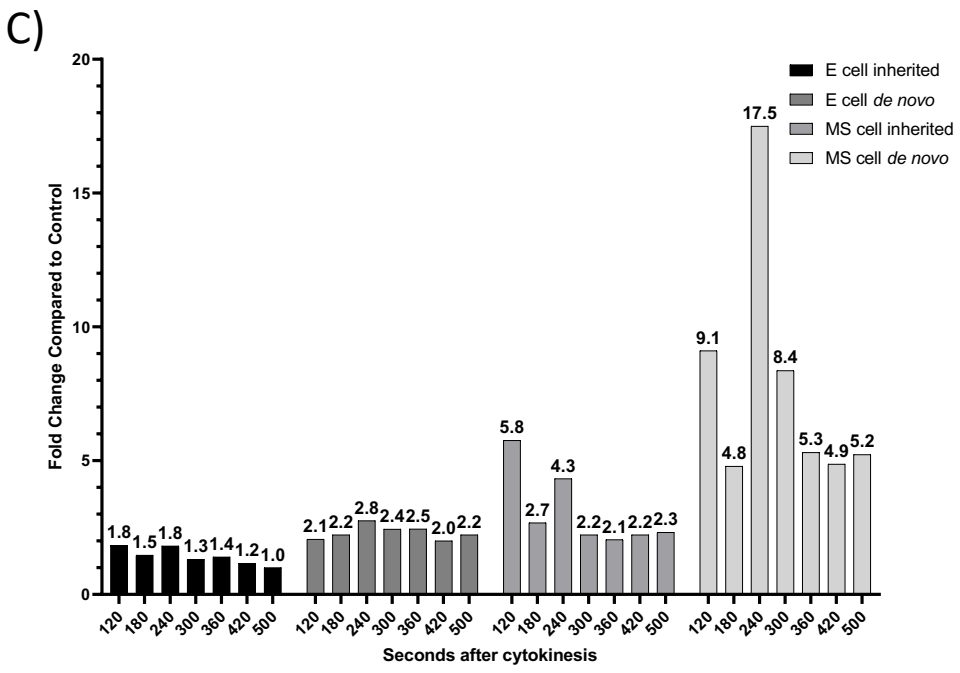
C)
E cell inherited
E cell de novo
MS cell inherited
MS cell de novo
Fold Change Compared to Control
Seconds after cytokinesis

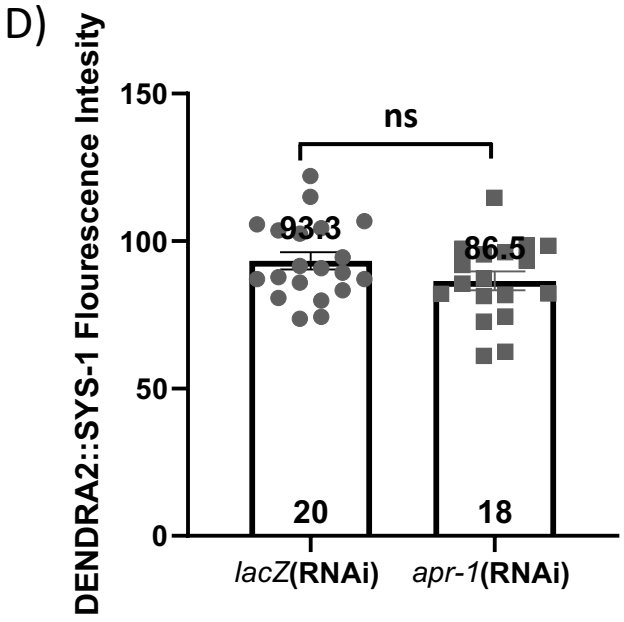
D)
ns
93.3
86.5
20
18
DENDRA2::SYS-1 Flourescence Intesity
lacZ(RNAi)
apr-1(RNAi)

Figure 7

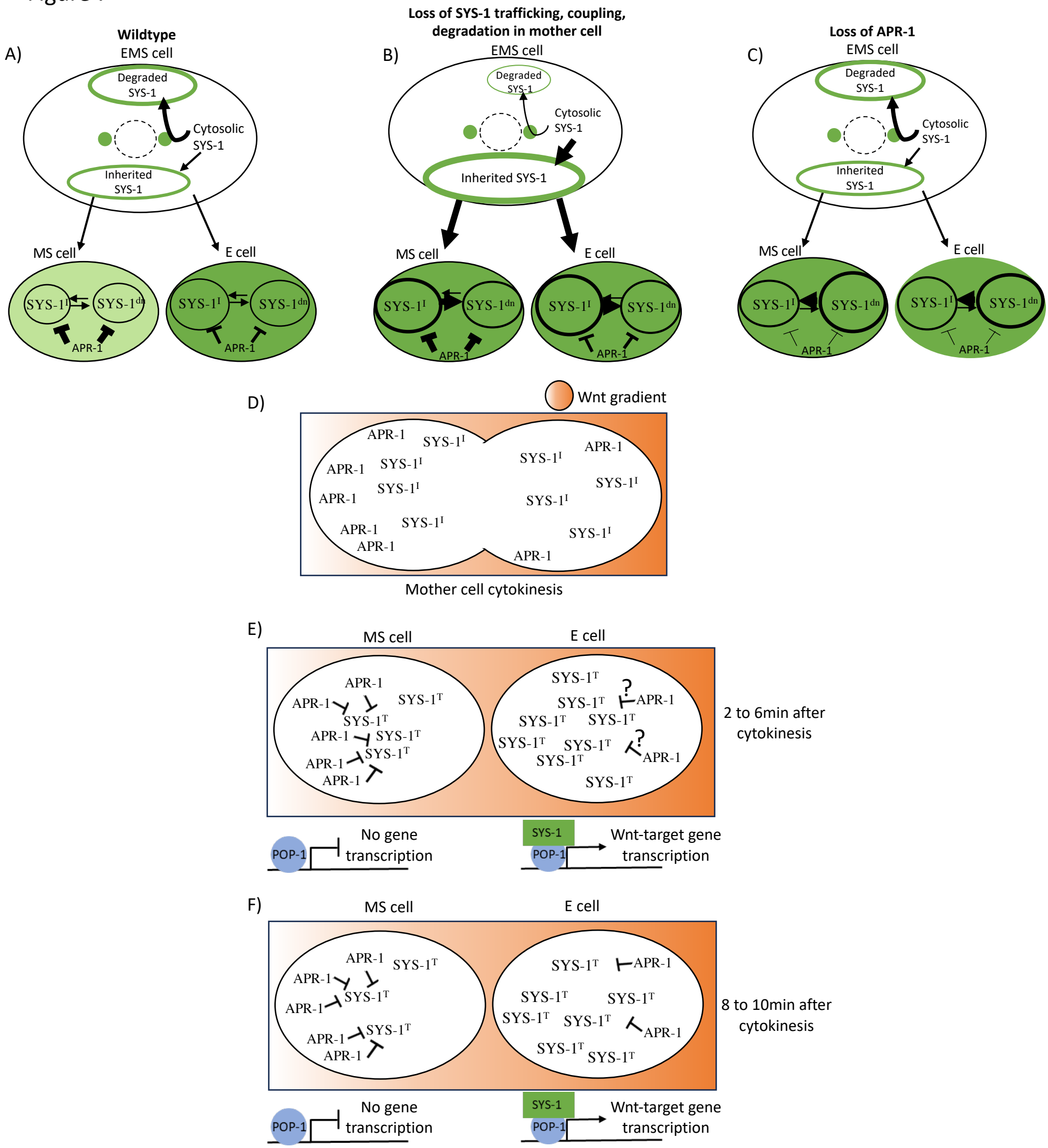
A)
Wildtype
EMS cell
Degraded SYS-1
Cytosolic SYS-1
Inherited SYS-1
MS cell
E cell
SYS-1I
SYS-1dn
APR-1
B)
Loss of SYS-1 trafficking, coupling, degradation in mother cell
EMS cell
Degraded SYS-1
Cytosolic SYS-1
Inherited SYS-1
MS cell
E cell
SYS-1I
SYS-1dn
APR-1
C)
Loss of APR-1
EMS cell
Degraded SYS-1
Cytosolic SYS-1
Inherited SYS-1
MS cell
E cell
SYS-1I
SYS-1dn
APR-1
D)
Wnt gradient
APR-1
SYS-1I
Mother cell cytokinesis
E)
MS cell
E cell
APR-1
SYS-1T
?
2 to 6min after cytokinesis
POP-1
No gene transcription
SYS-1
Wnt-target gene transcription
F)
MS cell
E cell
APR-1
SYS-1T
8 to 10min after cytokinesis
POP-1
No gene transcription
SYS-1
Wnt-target gene transcription